MID ATLANTIC BIGHT: COASTAL UPWELLING & THE OFFSHORE WIND ENVIRONMENT

By

SARAH MURPHY

A thesis submitted to the

School of Graduate Studies

Rutgers, The State University of New Jersey

In partial fulfillment of the requirements

For the degree of

Master of Science

Graduate Program in Oceanography

Written under the direction of

Travis Miles

And approved by

_____

_____

_____

New Brunswick, New Jersey

January 2021

ABSTRACT OF THE THESIS

Mid Atlantic Bight: Coastal

Upwelling & The Offshore Wind

Environment

by Sarah Murphy

Thesis Director:

Travis Miles

The Mid Atlantic Bight (MAB) is a unique environment that supports diverse ecosystems, contains complex oceanographic features, and is located near dense centers of human population. A key component of the MAB shelf that affects its ecosystems and coastal communities is the Cold Pool. This cold-water mass develops below the seasonal thermocline from remnant winter water and remains present in the mid to outer shelf throughout the summer. The Cold Pool is the source for coastal upwelling, which is focused upon in this thesis as a unique oceanographic feature of the MAB that has implications for stakeholder groups like fisheries and offshore wind. Upwelling is important to coastal regions around the world and is linked with hypoxic bottom conditions and influences atmospheric circulation in the MAB. Coastal Upwelling was previously defined by Glenn et al. (2004) as a difference between onshore and offshore

sea surface temperature (SST) of at least 2°C. Using this definition, we can describe coastal upwelling events, both in size and duration from satellite SST fields.

This study involved the use of newly available high resolution GOES-16 SST for the observation of coastal upwelling in the MAB. Locally focused cloud-correcting methods, referred to as the Spike Filter (SF), were developed for GOES SST in order to retain upwelling pixels. The Spike Filter (SF) method, greatly increased SST coverage of the coastal zone of the MAB by retaining more SST measurements than the aggressive cloud correcting algorithm (Quality Filter) provided by NOAA. DINEOF (Alvera-Azcárate et al. 2009) was then used to statistically gap-fill missing data to complete the GOES SST fields. GOES SF DINEOF SST approximately doubled the number of detected upwelling days compared to MUR SST. The longest upwelling event detected in GOES SF DINEOF persisted for over 17 days which is longer than the maximum outlier previously observed using 9 years of AVHRR measurements (Glenn et al. 2004). These observations suggest that MAB upwelling may be occurring more persistently, rather than as a series of short episodic events, and they can be more readily observed with continuous GOES SST data. Clear detection of the timing and duration of upwelling events is important as it provides estimates for ecological and physical responses in the MAB. GOES SST is valuable for the detection of upwelling in the MAB and should be adapted for application in ocean and atmospheric modeling.

GOES SF DINEOF SST was then used as part of an atmospheric analysis to test the sensitivity of the Rutgers Weather Research and Forecasting Model (RU-WRF) to different ocean surface boundary conditions. Three SST products, varying in resolution and their ability to capture upwelling, were chosen for this analysis. This analysis

demonstrated that there is a difference in RU-WRF forecasted wind speeds at a location in the NJ offshore wind energy using different SSTs during a week-long upwelling event. Forecasted wind speeds at turbine hub height varied in both the timing of wind speed changes and the total magnitude, which equate to differences in the potential wind power production for an offshore wind turbine. The accuracy of forecasted winds in this area affect the ability of the wind farm to correctly match electricity supply to grid demand. This analysis makes the case for further investigations over a longer time period that can be validated with newly available data such as the Atlantic shores LIDAR buoy to determine what SST provides the most accurate ocean conditions and wind forecasts.

Acknowledgements

First, I would like to thank my advisor, Travis Miles, for providing continued support and guidance throughout my time at Rutgers. His passion for research is infectious to those around him and was inspiring for me as a graduate student. I really appreciated having the opportunity to work with him and the research groups he involved me in both at Rutgers and at the University of Delaware. He provided constant direction for my research while also encouraging me to pursue my interests in climate change and renewable energy policy.

I would also like to thank my colleagues at Rutgers for all of contributions they have made to my research. Laura Nazzarro was extremely patient as I faced many challenges learning how to use Matlab. I truly could not have completed my thesis without her. I would also like to thank Joe Brodie for his contributions to the RU-WRF analyses, for all of the tutorials he put together, and for being such a friendly person.

Next, I would like to thank my committee members, Josh Kohut and Matt Oliver for providing advice throughout the development of my thesis. Both Josh and Matt were extremely helpful in meeting with me to review and provide edits for my paper submission. I really enjoyed getting to be a part of the University of Delaware satellite calls and I would like to thank James Simkins and Matt Shatley for all of their help with the GOES data.

I would like to acknowledge my friends from my C2R2 cohort and for Carrie Ferraro, Jeanne Herb, and Lisa Auermuller for being amazing instructors. This program was a huge part of my instructional time at Rutgers and I enjoyed learning more about climate change and applied science and being surrounded by graduate students from other

disciplines. I would also like to thank Johnny Lin for providing IT support and, more importantly, for being such a supportive friend on campus. Lastly, I would like to thank my friends, family, and Mark for their comfort and encouragement.

Acknowledgment of Previous Publications

Section 1.2 and portions of section 1.3 of the introduction of this thesis are part of a literature review completed for SCEMFIS, “Could federal wind farms influence continental shelf oceanography and alter associated ecological processes?” by the following authors: Travis Miles, Sarah Murphy, Josh Kohut, Sarah Borsetti and Daphne Munroe. The text and figure 2 included in this thesis reflects the contributions made by Sarah Murphy to this literature review. Chapter 2 of this thesis has been submitted for publication and is currently under review. This material represents the original work of the student with help from the following coauthors: Laura J. Nazzaro, James Simkins, Matthew J. Oliver, Josh Kohut, Michael Crowley, Travis N. Miles.

Table of Contents

List of Tables

List of Figures

Chapter 1

Introduction

1.1 Human interaction with the Mid-Atlantic Bight

The Mid-Atlantic Bight (MAB) is the coastal region extending from Cape Cod, Massachusetts to Cape Hatteras, North Carolina. The MAB a unique environment that supports diverse ecosystems and contains complex oceanographic features. Here, there is an overlap of human demand and valuable resources. For example, the commercial fishing industry in New Jersey leads in shellfish landings and provides the state with significant economic benefits (NJDEP 2005). The offshore wind industry is quickly expanding in the Mid Atlantic as the demand for renewable energy increases. These stakeholder groups will need to coexist over the shared resources of the Mid Atlantic Bight (MAB). They are interconnected in that fisheries rely on the health of the MAB ecosystem that offshore wind energy seeks to maintain, and the physical presence of offshore wind farms may impact fisheries operations.

An enhanced understanding of the offshore environment will ensure the resilience of the MAB ecosystem and stakeholder groups. The resilience of fisheries is linked to its ability to adapt to the changing environment. The efficiency of offshore wind will improve with an increased understanding of oceanographic and atmospheric conditions. Both groups are subjected to the unique ocean conditions of the MAB, the Cold Pool being a major driving feature of the physics and ecology of the region. These needs drive a motivation to learn more about the MAB and the features of the Cold Pool, which can

be accomplished through the use of advancing observational and modeling ocean technologies.

1.2 The Cold Pool

The Cold Pool is historically defined as the 8-10°C or colder bottom water occupied between the 0-100m isobaths from Georges Bank to Cape Hatteras beneath the seasonal thermocline. On average it is about 35m thick, representing 30% of the total volume of MAB shelf water (Pacheco 1988; Houghton et al. 1982; Voynova, Oliver and Sharp 2013; Glenn et al. 2004). Although typically defined as a pool of <10ºC water, the Cold Pool gradually warms from an average of about 7ºC in May to 10ºC in September, presumably due to heat fluxes through its surface and lateral boundaries (Lentz et al. 2017). The Cold Pool develops in the spring of each year, reaches peak volume in early summer (Chen et al. 2018), and is eroded in early fall of each year (Figure 1). Mechanisms proposed for the formation and maintenance of the Cold Pool by Bigelow (1933) and Houghton et al. (1982) suggest that the Cold Pool forms as remnant well-mixed winter water over the shelf, capped by stratification, fresh water runoff, and reduced wind mixing in spring (Lentz et al. 2003). The Cold Pool is a highly dynamic feature that varies in size and location within and among years (Figure 1), depending on a variety of oceanographic processes (Chen and Curchitser 2020). Seasonal Cold Pool evolution is central to structuring the MAB ecosystem. Intense ocean variability drives an equally variable ecosystem, from primary producers (Malone et al. 1988) to highly migratory fisheries throughout the region. Cold Pool waters are nutrient enriched and when advected coastward and upwelled toward the surface, stimulate rapid

phytoplankton growth as they are exposed to sunlight, sustaining high primary production (Voynova, Oliver and Sharp 2013). In addition, the Cold Pool provides important thermal refuge for many species, sustains fauna farther south than would be anticipated by its latitude, and regulates migratory behavior of fish.

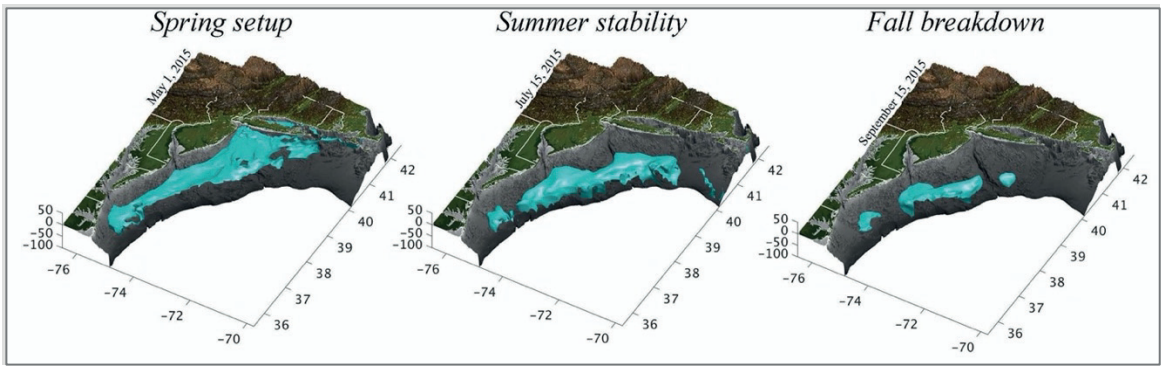

Figure 1. The seasonal footprint of the Cold Pool represented by ocean temperature imagery from the Espresso model. Three daily images from 2017, representative of each season, illustrate the 10ºC water mass spatially and at depth (m).

1.2.1 Spring Setup

In winter, MAB shelf water cools, reaching its lowest temperature in late February or early March (Pacheco 1988). Winter water is well mixed with a weak horizontal gradient toward warmer offshore water, and any weak vertical stratification is due entirely to salinity driven by freshwater input from estuaries along the coast (Castelao, Glenn and Schofield 2010). An additional upstream source of MAB shelf water originates in the Northern Labrador Sea and continually transforms as it transits south through the Gulf of Maine before entering the MAB. (Fairbanks 1982; Chapman and Beardsley 1989; Smith 1983; Mountain and Manning 1994; Wallace, Looney and Gong 2018). As these waters move south over Nantucket shoals, strong tides cause vigorous mixing before this cold denser bottom water spreads south into the MAB along the mid-shelf at approximately

$2cm \cdot s^{-1}$ (Chen et al. 2018). Additional studies indicate this remote supply of cold bottom water from the north helps to maintain and enhance MAB stratification throughout spring and into summer (Brown et al. 2015; Fairbanks 1982; Chen et al. 2018; Chen and Curchitser 2020). Throughout the spring setup, the Cold Pool interacts with adjacent water masses including the Gulf Stream water which can cause warm and salty intrusions along the MAB slope (Fogarty et al. 2007; Wallace et al. 2018).

The Cold Pool forms sometime between late March and May as surface heat fluxes increase and wind mixing from storm activity is reduced (Houghton et al. 1982; Lentz 2017; Bigelow 1933; Castelao, Glenn and Schofield 2010). During this time, a stratified water column develops with a warm and shallow near surface layer that caps off the cold bottom water (Chen and Curchitser 2020). The onset of vernal warming is irregular across the MAB and can be complicated by the cold and warm water intrusions summarized above (Pacheco 1988). Nearly half of the annual freshwater runoff in the MAB occurs in spring, which can further intensify the development of stratification, which isolates the Cold Pool from the warm surface waters (Castelao, Glenn and Schofield 2010; Pacheco 1988; Houghton et al. 1982). At its offshore edge, the Cold Pool is bounded by warmer, saltier slope water and the shelf-break jet, a narrow southward flowing current along the edge of the continental shelf (Linder and Gawarkiewicz 1998; Flagg et al. 2006; Lentz 2017).

1.2.2 Peak Summer Stability

Through summer, the thermocline strengthens due to surface heating and freshwater runoff, reaching a seasonal peak in July or August (Castelao, Glenn and Schofield 2010). At this peak, the average density difference across the pycnocline is as large as 4 kg/m3

(Castelao, Glenn and Schofield 2010), and surface-to-bottom temperature differences reach approximately 10^{o}C (Lentz 2017). From July to October, rapid warming of the Cold Pool occurs over Georges Bank, and more gradual warming occurs in central and southern MAB (Lentz 2017; Bigelow and Schroeder 1953; Houghton et al. 1982) due to heat fluxes in its surface and lateral boundaries (Benway and Jossi 1998; Chen 2018; Lentz 2017). Near the 60m isobath, maximum bottom temperatures are not reached until mid-November; however, warming is faster in shallower water due to a vertical turbulent heat flux from the thermocline to the Cold Pool (Lentz 2017). Here, seasonal heating extends to the bottom and maximum bottom temperatures can be reached in September. In general, the northern extent of the Cold Pool retreats 2.6 times faster than the southern extent due to horizontal advection of upstream warm water in Georges Bank and downstream advection at the southern edge (Chen 2018).

Throughout this stable summer Cold Pool peak, it is repeatedly acted on by wind events, gulf stream rings, bathymetric features, convective and advective mechanisms, and seasonal and interannual variations (Pacheco 1988). Under this extreme summer stratification, the Cold Pool is a relatively slow-moving feature with a long-term average flow in a season of 1-3 $cm \cdot s^{-1}$ southwestward in the alongshore direction. Throughout this slow migration down the shelf, the Cold Pool position varies in response to surface wind forcing. This movement can lead to seasonal ocean events along the coast. As an example, along shore winds will force the Cold Pool to slosh back and forth between the coast and shelf break. Movement toward the coast is called upwelling (driven by southwesterly winds) and movement away from the coast toward the shelf break is called downwelling (driven by northeasterly winds). Typical summer winds are either from the

Northeast (downwelling favorable) or Southwest (upwelling favorable.). During summertime periods of persistent upwelling favorable wind conditions, the Cold Pool is advected towards the coast as the surface layer moves offshore. In addition to being low temperature, these subsurface Cold Pool waters are nutrient enriched (Voynova, Oliver and Sharp 2013). Their advection coastward stimulates rapid phytoplankton growth as nutrient rich waters upwell toward the surface and are exposed to sunlight sustaining high primary production. The shoreward edge of the Cold Pool during the oscillations between upwelling and downwelling winds in the summer moves the onshore edge of the Cold Pool from the coast to as far as 75km offshore on time scales of days to weeks (Glenn et al. 2004). The occurrence of upwelling events is modulated by wind forcing, the location of the Cold Pool, the strength of coastal river plumes, and the occurrence of downwelling favorable winds during summer storms. This upwelled water can drive development of very large phytoplankton blooms that are advected offshore near the surface by wind (Shah, Mathew and Lim 2015). In addition, following colder winters, the most significant upwelling events have been observed suggesting severe cooling may result in a larger and/or colder Cold Pool (Glenn et al. 2004).

1.2.3 Fall Breakdown

During the fall, an increase in the frequency of strong wind events and decreasing surface heat over increasingly shorter daily daylight hours leads to enhanced vertical mixing that ultimately breaks down the Cold Pool (Gong, Kohut and Glenn 2010; Bigelow 1933; Lentz et al. 2003; Lentz 2017; Castelao, Glenn and Schofield 2010). In late summer, the thermocline deepens near the coast and begins mixing downward, increasing bottom temperatures (Pacheco 1988). Vertical mixing can also be induced through internal wave

breaking in the region of the pycnocline, and intrusions of warm-salty slope water in the bottom boundary layer which may be associated with upwelling favorable winds (MacKinnon and Gregg 2005; Lentz et al. 2003). Each successive storm weakens thermal stratification, reducing stability and allowing for more mixing until it becomes vertically uniform at 10-15ºC and the seasonal Cold Pool disappears. This breakdown typically occurs within ~1 month after surface temperatures reach a maximum near the end of summer (Ketchum and Corwin 1964). Recent work has identified the importance of fall transition storms that can rapidly mix the water column. Late season tropical storms or extra-tropical cyclones, often referred to as fall transition storms can lead to abrupt erosion of the Cold Pool over a few days, or even hours depending on storm strength and remaining water column stability (Seroka et al. 2016; Glenn et al. 2016; Miles et al. 2017). Therefore, timing of Cold Pool breakdown varies significantly each year and has been documented to occur anytime from mid-September to November (Lentz 2017; Lentz et al. 2003; Chen 2018; Bigelow 1933; Pacheco 1988).

1.3 Offshore Wind

The offshore wind industry is expanding rapidly along the east coast of the US as the demand for renewable energy has increased. States have set aggressive renewable energy goals with offshore wind being a major contributor to those goals. For example, New Jersey currently has a goal of 50% renewable energy by 2030, consisting of 7500MW of offshore wind by 2035 (Murphy 2019). These renewable energy goals drive policy mandates and reduce the overall cost of offshore wind is the US. Offshore wind is a regionally uniform resource that is economically viable and located in areas of high electricity demand (Kempton et al. 2007). The low surface roughness of the ocean allows

for the winds above the ocean to be faster and less variable in time than onshore, as indicated by the higher persistence of wind speeds above turbine cut-in speeds at offshore sites (Pryor and Barthelmie 2001). New Jersey is ideally geographically situated for offshore wind development and offers various assets to the industry. New Jersey has a total of 7,477km^2 area of state waters with a minimum average wind speed of 7m s^{-1} (DOE 2016). Its strategic east coast central location, long coastline, shallow continental shelf, steady wind resource, and an educated workforce is appealing (FRI 08 2018).

Once in place, the wind farms have a lifespan of 20-30 years and it is anticipated that more will be developed throughout the east coast. There is currently only one small operational offshore wind farm in the US, leaving much uncertainty in the future of offshore wind. The Mid Atlantic has extremely unique environmental characteristics that the industry has yet to face that must be understood to properly assess the offshore wind resource. The Cold Pool has an influence on surrounding atmospheric conditions by affecting the exchange of energy between the ocean and atmosphere during events like storms and coastal upwelling. Due to these reasons, it is vital that the Mid-Atlantic physical and ecological environment be thoroughly explored and understood.

As seen in Figure 2, there is significant overlap between the location of the Cold Pool and the location of offshore wind lease areas. The Cold Pool has the largest spatial extent in June-August and the greatest stratification in July. The timing of the formation and breakdown and the area extent of the Cold Pool is highly variable. As shown in Figure 2, the location of the Cold Pool occupies closer to shore in May and cuts across the location some of the offshore wind lease areas like off of NJ in August as it moves further offshore. By the time of the typical breakdown of the Cold Pool, in September

and October, there is very little overlap between the Cold Pool and the offshore wind lease areas. As shown in Table 1, more than half of the offshore wind lease areas off of Massachusetts, New York, New Jersey, and Maryland, are underlain by the Cold Pool in May and June. The Cold Pool remains present in the majority of the lease areas off of Massachusetts, New York and New Jersey even later in the season through August.

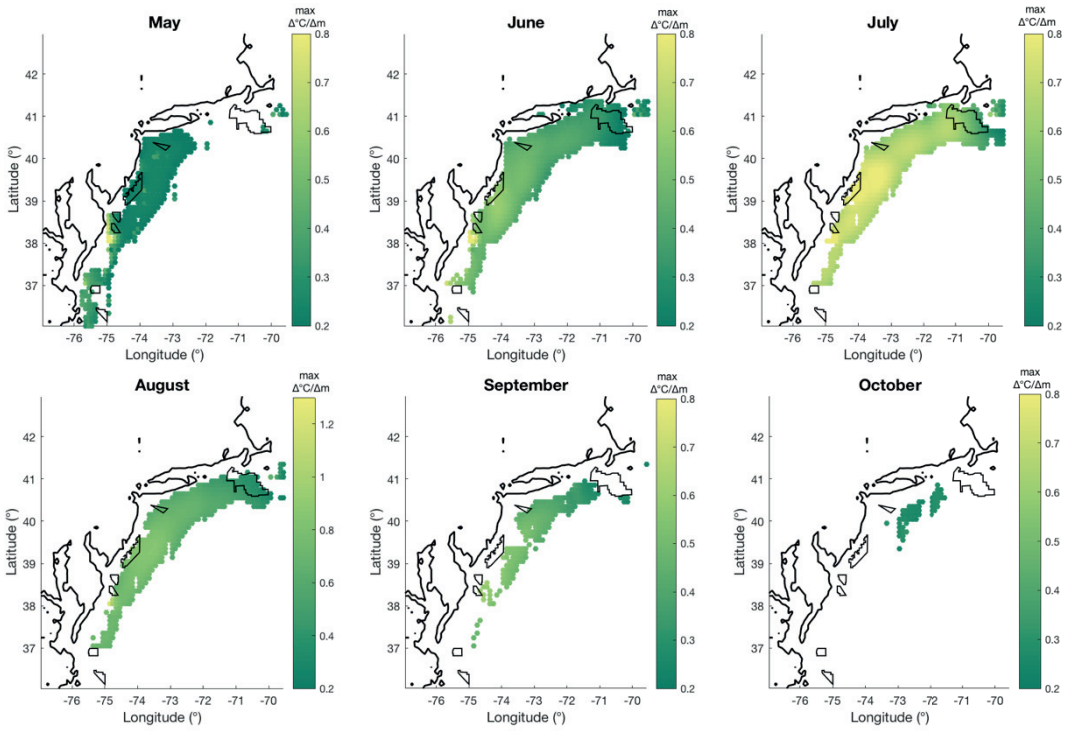

Figure 2. Average spatial extent of the Cold Pool by month with offshore wind lease areas outlined in black. Colored pixels indicate where locations where the bottom water is <10ºC and stratified water exists (>=.2ºC/m) and is qualified as the Cold Pool. The Cold Pool. The color of the circles indicates the strength of the maximum stratification (ºC/m). Data are the statistical mean of 2005-2012 Northwest Regional Climatology data at 1/10º

grid accessed from World Ocean Atlas at:
https://www.nodc.noaa.gov/OC5/regional_climate/nwa-climate

Table 1. Percentage of Offshore Wind lease Area Occupied by the Cold Pool. Calculated as the number of Cold Pool pixels out of the total number of ocean pixels in each lease area.

Lease Areas	May	June	July	August	Sept.	October	Total Pixels
Mass. / RI	6.3	**91.7**	**100**	**72.9**	0	0	48
New York	**100**	**100**	**80**	**80**	20	0	5
New Jersey	**89.5**	**73.7**	**63.2**	**68.4**	0	0	17
Delaware	**60**	40	0	0	0	0	5
Maryland	**100**	**66.67**	**50**	16.7	0	0	6
Virginia	11.1	0	0	0	0	0	9
North Carolina	0	0	0	0	0	0	6

These figures demonstrate the importance of improving the understanding of the Cold Pool for the offshore wind industry as it drives the surrounding physical, ecology, and atmospheric conditions. The Cold Pool occupies the majority of the MAB offshore wind lease areas at various points throughout the summer during which upwelling events typically occur. Therefore, offshore wind areas may be impacted by the oceanographic and atmospheric conditions of upwelling events in the MAB.

1.4 Thesis scope

The goal of this thesis is advance our understanding of the mechanistic link between the Cold Pool and offshore winds. In order to do this, newly available Geostationary Operational Environmental Satellites (GOES-16) SST is used to observe MAB coastal upwelling and as SST input for wind forecasting. This thesis is aimed at demonstrating the importance of including newly developed technology in ocean observation and modeling. Coastal upwelling is an important feature of the MAB, and is linked with the highly dynamic conditions of the Cold Pool and overlying atmosphere. Upwelling events

have been shown to influence atmospheric and ecological conditions of the MAB and are of interest to both fisheries and the offshore wind industry, amongst other stakeholders. Satellite SST is an important tool in observing coastal upwelling events and is assimilated into ocean and atmospheric modeling. The use of GOES SST imagery may provide more realistic ocean conditions which is a critical component of wind forecasting in the offshore environment.

The second chapter includes the development of quality control and gap-filling methods applied to GOES SST to create a complete data set that retains upwelling pixels. This chapter also demonstrates the importance of high-resolution upwelling-retained SST in improving the observation of upwelling in the MAB. The second chapter is the main focus of this thesis in that it provides a detailed analysis of the observation of coastal upwelling observation using GOES SST compared to other SST products. The third and final chapter is a brief analysis using the GOES SST data set as input in RU-WRF to demonstrate the sensitivity of wind forecasting and to various SST inputs. This thesis demonstrates the importance of using new oceanographic technology to improve our understanding of the MAB and ensure the resilience of existing stakeholder groups.

Chapter 2

Persistent Upwelling in the Mid-Atlantic detected using Gap-Filled, High-Resolution Satellite SST

2.1 Abstract

This study applied a cloud correction technique and DINEOF to gap-fill newly available GOES-16 SST for the observation of upwelling in the Mid Atlantic Bight (MAB). Upwelling is important to coastal regions around the world and is linked with hypoxic bottom conditions and influences atmospheric circulation in the MAB. During the 2019 upwelling season, the Quality Filter (QF) provided to cloud correct GOES SST consistently removed upwelling pixels, resulting in ~15% MAB coastal SST coverage. The Spike Filter (SF) method increased MAB coastal SST coverage to 30% and maintained overall accuracy. GOES SF DINEOF SST approximately doubled the number of detected upwelling days compared to MUR SST. The longest upwelling event detected in GOES SF DINEOF longer than the maximum outlier previously observed using 9 years of AVHRR measurements (Glenn et al. 2004). The number of upwelling events observed in this study, ~3, also falls on the low end of the range of the total events per summer previously observed (Glenn et al. 2004). This suggests that MAB upwelling may be occurring more persistently, rather than as a series of short episodic events as previously thought. Clear detection of the timing and duration of upwelling events is important as it provides estimates for ecological and physical responses in the MAB. GOES-16 SST has the potential to improve upwelling detection in the MAB and should be further studied for application in ocean and atmospheric modeling.

2.2 Introduction

Upwelling affects the ecology and dynamics of coastal regions throughout the world (Schwing et al. 1996). The frictional stress of wind on the ocean causes surface water to be transported offshore and be replaced by cold, nutrient rich bottom water. The introduction of the nutrient rich bottom water in the euphotic zone stimulates primary production, drives food webs and sequesters carbon dioxide. Upwelling is responsible for some of the world's most highly productive fishing regions including the coastal waters of Peru and California (Narayan et al. 2010). During the springtime in the Mid Atlantic Bight (MAB), cold remnant winter water is surrounded by the warming surface water and developing thermocline and by the warmer offshore slope water, creating an isolated area of deep winter water known as the Cold Pool (Lentz 2017). Throughout the summer, the Cold Pool remains along the bottom of the mid shelf. If persistent southerly winds develop, cold bottom water is upwelled to the surface along the coast as the warm surface water is driven offshore (Castelao et al. 2010). During an upwelling event, cold SST can be seen along the coast and extending offshore of recurrent upwelling centers off New Jersey and the Delaware Bay (Figure 3).

In the MAB, summertime upwelling events are known to produce large coastal blooms and are linked with hypoxic bottom conditions resulting in major financial losses for the shell fishing industry (Glenn et al. 2004). Upwelling causes the input of cold, nutrient rich water to the surface driving phytoplankton blooms and high concentrations of particulate organic matter in the water column. This organic matter sinks to the bottom and is broken down through microbial respiration, and can deplete 75% of the oxygen

concentration in the bottom water off the coast of NJ. According to Glenn et al. (2004), increased phytoplankton concentrations occur immediately upon the onset of upwelling conditions and the total number of upwelling days provides an estimate of the amount of time that the enhanced organic material is deposited in the upwelling center. Similar effects have been seen in Delaware Bay upwelling events (Voynova et al. 2013). These findings reinforce the importance of clear detection of the timing and duration of upwelling events, which can cause major financial loss for fisheries. Satellite data, along with other observations, is integrated into ocean models in the Mid-Atlantic to support products that have been shown to improve habitat models (Oliver et al. 2013). In the Mid Atlantic coastal ocean, SST and chlorophyll-a fronts, along with other hydrographic processes, influence habitat associations for several species (Manderson et al. 2011). For example, in Oliver et al. (2013), Atlantic sturgeon were observed in shallow, well-mixed, warm freshwater associated with a Delaware Bay water mass. Knowing the timing and location of this endangered species can inform management recommendations to reduce interactions with fisheries.

In addition to ecological impacts, upwelling can impact atmospheric processes. Sea-breeze circulation develops due to differential heating of air over land and sea. The resulting pressure gradient causes low-level air to move from the sea to land with a return from aloft. By increasing the land-sea thermal gradient, upwelling has been shown to influence sea breeze circulation (Seroka et al. 2018). During the simulated upwelling event in the MAB, the sea breeze began earlier and was more intense. Upwelling enhanced the sea breeze near the surface and strengthened the return flow aloft. Upwelling produced colder air above the surface and warmer air above that at ~400-

700m. Seabreeze enhancement due to upwelling was observed up to ~750m with return flow enhancement >750m. The occurrence of upwelling and sea breeze in the MAB coincide with electricity demand peaks, making it significant for offshore wind resource assessment. Due to the impact on both the fishing and renewable energy industries, amongst other stakeholders, it is important that upwelling can be readily detected in the MAB.

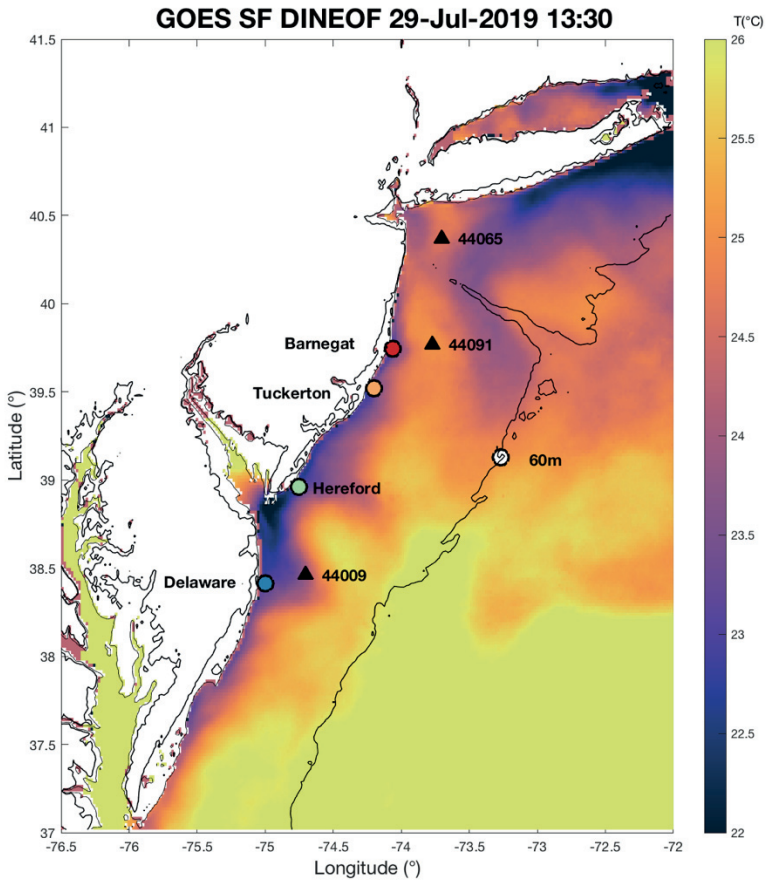

Figure 3. GOES SF DINEOF reconstructed SST image of the Mid Atlantic Bight study area. Bathymetry contours are drawn for the coastline, 0m, and at -60m offshore. The

locations of buoys used for validation (black triangles), the recurrent upwelling centers (colored circles), and the 60m offshore reference point (white circle) are shown.

Upwelling cold water can be identified by measuring sea surface temperature (SST) in coastal regions. Prior to the 1970s, SST measurements were limited to in situ retrieval from buoys, boats, and on shorelines (Minnett 2019). These methods require rigorous sampling and have highly limited spatial and temporal resolutions and coverage. In the MAB, the absence of National Data Buoy Center (NBDC) buoys in the recurrent upwelling centers make it likely that only large events that extend further offshore are traceable by long-term buoy measurements. Satellite measurement of SST has resulted in major advancements in oceanography and atmospheric sciences. Thermal infrared satellites measure SST by detecting the radiation emitted by the motion of ocean particles, which varies with temperature (Wentz et al. 2005). Thermal infrared instruments used for measuring SST include Moderate Resolution Imaging Spectroradiometer (MODIS), Advanced Very High Resolution Radiometer (AVHRR), Geostationary Operational Environmental Satellite Imager (GOES), and others. However, satellite measurements are limited because they are often obscured by clouds, require atmospheric corrections, and have infrequent return periods (Maurer 2002).

The GOES-R satellite, launched on November 19th, 2016, greatly improves upon the spatial and temporal resolution of previous GOES systems and other available satellites SST products (Schmit et al. 2017). High resolution GOES images have the potential to provide greater SST coverage of coastal regions and small-scale oceanographic processes. These measurements are important for studying coastal upwelling events, which can evolve over hours to a few days. Upwelling events in the MAB are highly

variable in size and duration and have been observed to occur for up to half of the days in the summer season (Glenn et al. 2004). The frequency and variability of this ocean phenomenon makes it difficult to study without the availability of data with high spatial and temporal resolution, making the newly available hourly GOES-16 satellite technology very valuable for analysis of upwelling. GOES provides global SST coverage in hourly composited images whereas polar orbiting satellites provide global coverage twice per day, per satellite and can be collected when the satellite is within range of a receiving station.

Despite the improvement to SST data provided by the addition of GOES, appropriate cloud-correction is a persistent issue seen in satellite data. Data quality control measures designed to remove corrupted cloudy pixels from satellite measurements often also remove cold upwelling water. A technique known as the 'coldest-dark-pixel' composite (Glenn et al. 2016) has been developed to retain upwelling pixels for AVHRR SST in the MAB but has not yet been developed for GOES. SST considered good quality by the data quality flag (QF) developed for GOES is effective at removing cloud pixels but has been observed to remove cold coastal ocean pixels throughout upwelling events (Shabanov et al. 2010). This study proposes a technique involving a series of quality control tests and SST reconstruction to closely examine coastal upwelling in the MAB. Having a complete and robust SST dataset is not only important for understanding oceanographic processes, but can also provide insight for coupled ocean-atmosphere phenomena across global and local scales.

2.3 Methods

The GOES hourly SST product used in this study is derived from observations made by the NASA Geostationary Operational Environmental Satellite 16 (GOES-16) satellite (Mission Overview). GOES-16 is an advanced geostationary satellite offering high resolution atmospheric, oceanic, solar, and space-weather data via multiple state-of-the-art instruments. After launching in November 2017, GOES-16 underwent multiple calibrations, validations, and testing as it drifted towards its operational location at 89.58 W above the equator. In December 2017, GOES-16 was announced as operational and succeeded GOES-13 to become the GOES-East satellite. The primary instrument aboard the satellite is the Advanced Baseline Imager (ABI) which has 16 spectral bands equipped with the ability to scan full-disk (Western Hemisphere) at 15-minute intervals and 0.5-2.0 km spatial resolution. Multiple products have been derived from the ABI bands since the satellite has become operational. The primary product used for this study is sea surface temperature (SST). The SST product provides key ocean temperature information at full-disk spatial resolution and hourly temporal resolution and can be accessed at https://podaac.jpl.nasa.gov/. Summary information on the GOES-16 SST product is provided in Table 2. The algorithm responsible for producing GOES-16 SST is the Advanced Clear-Sky Processor for Oceans (ACSPO). The ACSPO requires ABI spectral bands 7 (3.9 microns), 11 (8.5 microns), 13 (10.35 microns), 14 (11.2 microns), and 15 (12.3 microns). These ABI inputs are used in conjunction with ancillary global weather data, ancillary Reynold's SST fields, ABI cloud and ice masks, and ABI clear-sky brightness temperatures to create the SST data. Extensive quality control is performed on each pixel of SST data which involves significant validation comparisons

to existing operational SST products and in-situ buoy observations. The output includes multiple variables which include SST and Data Quality Flags (DQF) for each pixel.

This data is uploaded in near-real-time to a publicly accessible Google Bucket. The University of Delaware Ocean Exploration, Remote Sensing and Biogeography Laboratory (ORB Lab) extracts the GOES-16 SST data in real-time via this Google Bucket and performs a reprojection of the spatial dataset at 2.0 km resolution, which they make publicly available on the ORB Lab databases at: http://basin.ceoe.udel.edu/thredds/. In this study, SST from the ORB lab database is extracted for the Mid Atlantic Bight within -77°W to -72 °W and 37°N to 42°N.

The GOES ABI processing system uses a preliminary cloud masking and subsequent Quality Control (QC) test to determine usable cloud-free ocean pixels for SST retrieval (Ignatov 2010). First, the ABI Cloud Mask identifies cloudy pixels which are not considered for use by the SST algorithm and is designed to minimize the discarding of potential good data. Next, the remaining pixels, which may still have significant cloud contamination, are annotated by the Data Quality Flags (DQF) into four categories: "Good," "Degraded," "Severely Degraded." and "Poor." The QC tests observed Brightness Temperature (BTs) for consistency with the Community Radiative Transfer Model (CRTM) which uses Ancillary Global Forecast System and Optimal Interpolation SST data as input (Mission Overview). SST flagged as "Optimal" by the DQF was retained for the GOES Quality Filtered SST. This strategy of separate preliminary cloud masking and subsequent data quality flags suggests the development of individual quality control products. Because cold coastal upwelling SST pixels are often removed by global quality flagging methods in the Mid Atlantic Bight (Glenn et al. 2004) the Spike Filter

(SF) method was designed to retain coastal upwelling SST pixels and applied to un-flagged GOES hourly SST.

The SF method is designed to further quality control SST by detecting sudden changes in temperature due to the presence of clouds, which typically persist for shorter time periods than coastal upwelling. The National Buoy Data Center (NBDC) quality control measures use similar time continuity and range limit checks for temperature and are described in further detail in the NBDC Technical Document 09-02 (NBDC 2009). The SF method includes the following four sequential steps: 1. Rate of SST change 2. Minimum SST threshold 3. Comparison to recent SST 4. SST bias correction. First, for each SST pixel, any change in temperature per pixel greater than 1°C/hour is removed, as surface ocean cooling rates are highly unlikely to exceed this threshold. Glider observations demonstrated that during a strong hurricane event, the surface ocean cooled at a rate of .5 degrees per hour in this region (Glenn et al. 2016) representing a likely upper bound for cooling from ocean processes in this region. Next, any SST below 12°C was removed. SST is not expected to be below 12°C in this region in the summer upwelling season. A climatology study which used 150 years of observations found the mean monthly SST value for the MAB from June-September to be 18-23°C (Richaud et al. 2016). In addition, upwelling studies observed a minimum SST of ~16°C along the coast of New Jersey (Glenn et al. 2004) and in the Delaware Bay (Voynova et al. 2013) during upwelling events. Next, any data more than 2 standard deviations outside a moving 7 day per pixel average was removed. Lastly, the bias correction was applied to GOES SST that had passed the previous three steps of the SF method. Bias was calculated as the difference between buoy SST and GOES SST matched to the buoy

locations and times of measurement. These values were calculated at NBDC buoys 44025, 44089, 44091, 44009, and 44065 (Figure 4) and then averaged for the entire time period. This analysis included additional buoys not used for validation to complete the bounding area. The averaged biases were: 44089: 0.1502, 44025: 0.2884, 44065: 0.2090, 44009: 0.3461, and 44091: -0.0198 ˚C. These values were placed in the GOES spatial domain at each of the corresponding buoy locations and then interpolated across the entire domain using inverse distance weighting interpolation (Figure 4). The interpolated grid of bias values was then added at every GOES SST pixel for the entire time period.

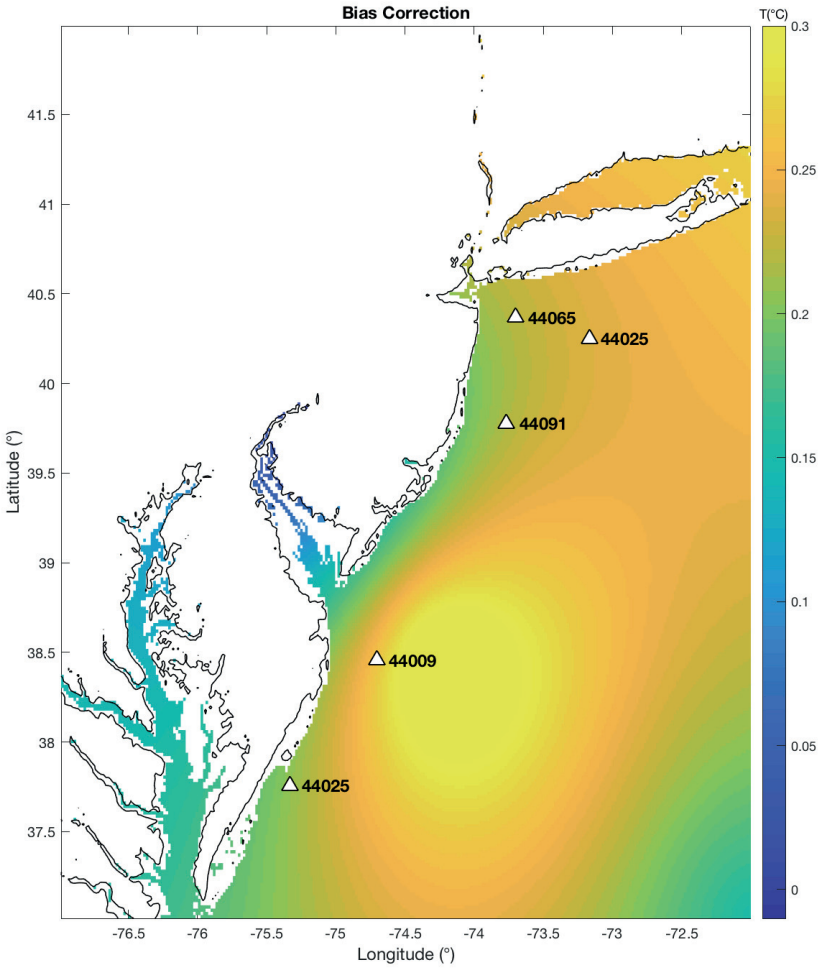

Figure 4. Bias correction applied to GOES SF Data based on averaged bias of GOES to buoy SST for the summer time period using Inverse Distanced Weighted Interpolation.

The GOES SF SST was then reconstructed using Data Interpolating Empirical Orthogonal Functions (DINEOF) (Alvera-Azcárte et al. 2009). Validation studies of DINEOF used for oceanographic data sets demonstrate robust results containing realistic and reliable ocean features. DINEOF is a technique that calculates missing data from an optimal number of Empirical Orthogonal Functions (EOF) obtained by cross-validation. This analysis ensures that the reduced variables represent a large fraction of the original variability of the data (Alvera-Azcárte et al. 2009). In the DINEOF algorithm, the

temporal and spatial average of the original dataset is removed and the first EOF mode is calculated using Singular Value Decomposition to estimate the missing data. This process is repeated until convergence is obtained for the estimated values for each EOF mode for the desired maximum amount of modes. Once the optimal number of EOF modes are determined, the reconstruction is performed again for those modes. This technique was performed on the SST dataset which contained 276 X 278 pixels and 2255 images. Final spatial size after excluding land points was 34876 points and contained an average of 66.29% missing data. DINEOF reconstruction was performed using the entire data set with a maximum of 20 EOF modes computed. The reconstruction parameter was set so that DINEOF reconstructed the entire matrix using the EOF base to avoid cold spikes at cloud edges and other sources of noise in the original matrix. The covariance matrix was filtered prior to reconstruction using an alpha value of 0.01 (the strength of the filter) and a Numit value of 1500 (the reach of the filter), selected to filter frequencies higher than 24 hours out of the data set. The Numit value was fine-tuned, similar to the methods used by A. Alvera-Azcárte et al. (2009) and 1500 was determined to provide the most accurate reconstruction while retaining the upwelling signal.

GOES SF SST and GOES SF DINEOF were validated against NBDC buoy SST. Buoys located in the MAB and inshore of the 30 m isobath were chosen for validation to focus on known upwelling regions. These included 44065 (New York harbor entrance, 40.369 N 73.703 W) 44009 (southeast of Cape May, 38.457 N 74.702 W), and 44091 (Barnegat, 39.778 N 73.769 W) (Figure 3). The root mean square (RMS) error: satellite minus buoy, model bias: mean satellite minus mean buoy, CRMS: (satellite minus mean

satellite) minus (buoy minus mean buoy), and total count: number of data available for comparison.

Additional SST products were chosen for comparison: MUR and AVHRR. MUR is a global product that provides daily SST images created from observations from several instruments and climatology at .01° latitude x. 01° longitude resolution. The AVHRR product chosen for analysis in this study is a global product that provides twice daily composited images from its polar-orbiting satellite passes at .05° latitude x .05° longitude resolution. These products were chosen because they are readily accessible global SST products that demonstrate the current ability of both satellite SST and gap-filled SST to detect upwelling in the MAB

2.4 Results

2.4.1 Satellite Observations

Hourly GOES SF DINEOF improved SST coverage of the Mid-Atlantic Bight for the time period studied when compared to twice daily composited AVHRR and daily MUR SST by providing more SST measurements at a high resolution and acceptable accuracy (see Table 2 for SST product details). As shown in Figure 5, the high spatial resolution of GOES allows it to better capture the complexity of ocean features in the region, while AVHRR SST contains coarser detail and the shape of the coastal upwelling water is less defined, and MUR SST appears to smooth the details of ocean features as well as underestimate the coldness of the upwelling SST. In the GOES Spike Filtered image, which is used for the GOES SF DINEOF reconstruction, both the offshore extent of upwelling and near shore pixels are well defined. GOES-16 also has a higher temporal resolution and contains hourly images as opposed to the twice daily composited AVHRR

product and daily composited MUR product, and GOES SF DINEOF provides ~17 times the number of AVHRR and MUR SST pixels for each buoy (Table 3). The GOES SF DINEOF SST has a comparable RMS error to the MUR filled in product and significantly lower RMS error than AVHRR (Table 3).

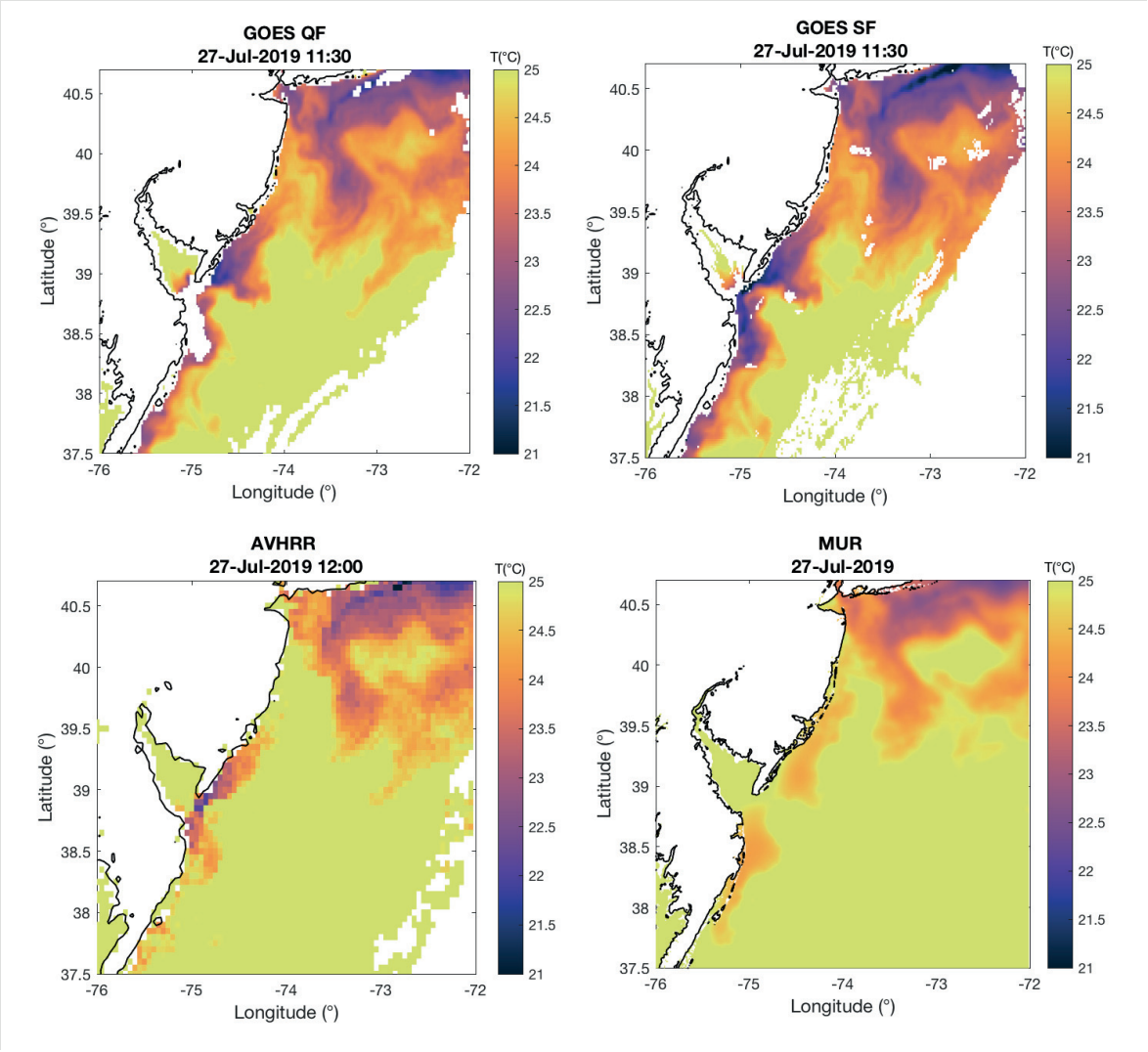

Figure 5. SST during an upwelling event on July 27, 2019 from the various SST products used for analysis. Images are shown on the top row: GOES QF and GOES SF and on the bottom row: AVHRR, and MUR.

Table 2. Satellite SST summary information for SST products used in analysis: MUR, AVHRR, and GOES-16.

	MUR	AVHRR	GOES-16
Satellite	observations from several instruments and climatology	Polar-Orbiting	Geostationary
Source	GHRSST L4	GHRSST L3C	L2+
Coverage	Global	Global	-77°W to -72 °W 37°N to 42°N
Spatial Resolution	0.01 degrees (Latitude) x 0.01 degrees (Longitude)	.05 degrees X .05 degrees	.5-2.0 km
Temporal Resolution	Daily	Twice Daily	Hourly
Processing	GDS version 2	Multispectral algorithm and bias correction	ACSPO
Target Accuracy	<0.4 K	<.4K	1 K
Time Span	2002-Jun-01 to Present	2016-Jan-06 to Present	2017-Dec-15 to Present
Platform/ Sensor	Aqua / AMSR-E Aqua/ MODIS InSitu/ InSitu, NOAA-19/ AVHRR-3 Terra/ MODIS CORIOLIS/ WINDSAT GCOM-W1 / AMSR2	MetOp-B/ AVHRR-3	GOES-16/ ABI

2.4.2 GOES Inter-product comparisons

As an example, Figure 5 compares how various SST products capture an upwelling event on July 27, 2019. The GOES Quality Filtered image is missing most of the cold SST off the southern tip of NJ and the Delaware Bay. Because the GOES default quality filter consistently flagged upwelling SST pixels as severely degraded, this was a persistent

complication observed throughout upwelling events in this study and in previous upwelling studies (Glenn et al. 2004; Kohut et al. 2004). Upwelling SST was also missing from AVHRR and MUR SST collected the same day, unlike the data filtered using the SF method which effectively removed cloudy data offshore while retaining coastal upwelling SST pixels in the Delaware Bay region. When applied to the entire time period, the SF improved coverage in the critical upwelling zone along the coast of NJ and Delaware (Figure 6), calculated as the number of timestamps per pixel containing SST data out of the total images used for this study. GOES QF SST provided low coverage along the coast, with SST measurements ~15% percent of the summer. GOES SF SST increased coverage in the coastal region to ~30% and was comparable to the percent coverage in the surrounding area offshore.

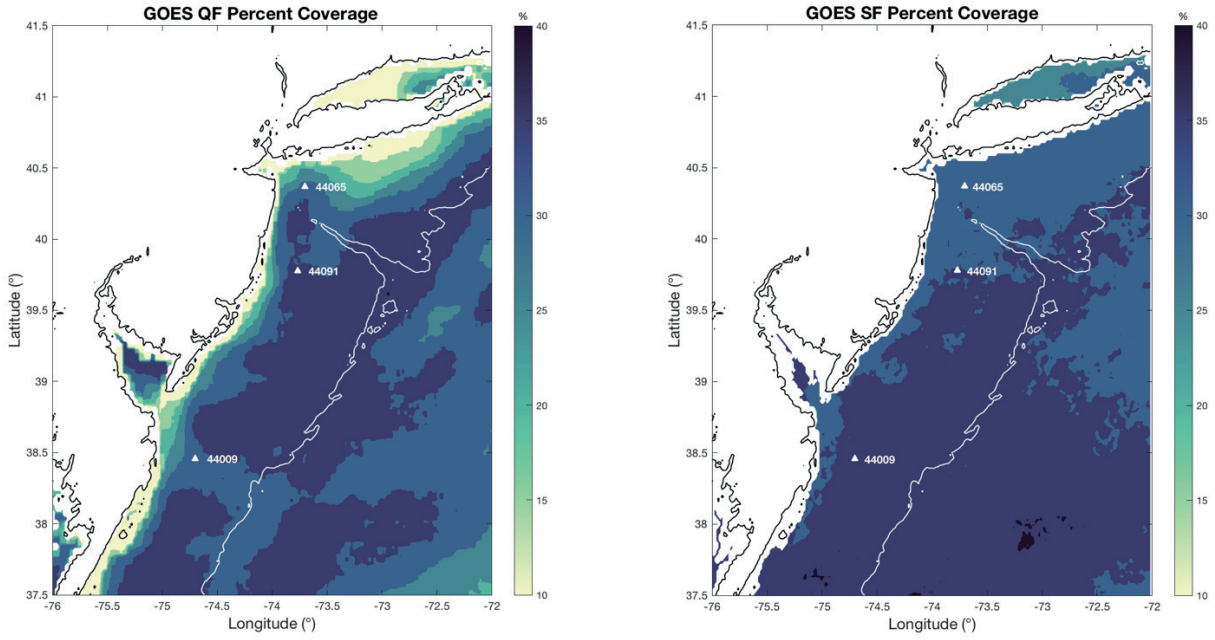

Figure 6. Percent of GOES SST (non-NaN) data available per pixel for summer time period (June 1-September 20) for GOES Quality Filtered (left) and the Spike Filtered (right).

GOES SST was validated for accuracy against regional NBDC buoy SST measurements and is presented in Figure 5 and as summary statistics in Table 3. At the location of each buoy, GOES Quality Filtered (QF), GOES Spike Filtered (SF) and GOES SF DINEOF SST was extracted and compared to the buoy SST measurement made at that time. The SST extracted from all three GOES data sets accurately match the overall trends in SST observed at buoy 44091 (Figure 5). GOES SST data contains early summer warming and late summer cooling observed by the buoy. In addition, the high quantity of GOES SST measurements detail smaller processes like diurnal cycles. The SF method is less conservative than the QF and occasionally allows in SST pixels that are colder than the buoy SST observed. However, the SF maintains the accuracy of GOES and GOES SF has a lower average RMS error than GOES QF, except at buoy 44091 where it exceeds QF RMS only by .14 of a degree, well within the 1-degree target accuracy of GOES SST. The SF filter preserved more data than the QF filter at each of the three buoys even though all three buoys are located outside of the coastal upwelling zone which displayed the most drastic improvement in coverage (Figure 6). Buoy 44009 was the most likely to possibly include upwelled water (Figure 3) and also had the greatest improvement in both coverage and RMS using the SF method. The bias correction applied to GOES SF SST reduced the warm bias at from 0.2090 to -.012 at buoy 44065 and from 0.3461 to .083 at buoy 44009.The SF filter improved coverage of the upwelling zone and maintained accuracy for the limited time period studied.

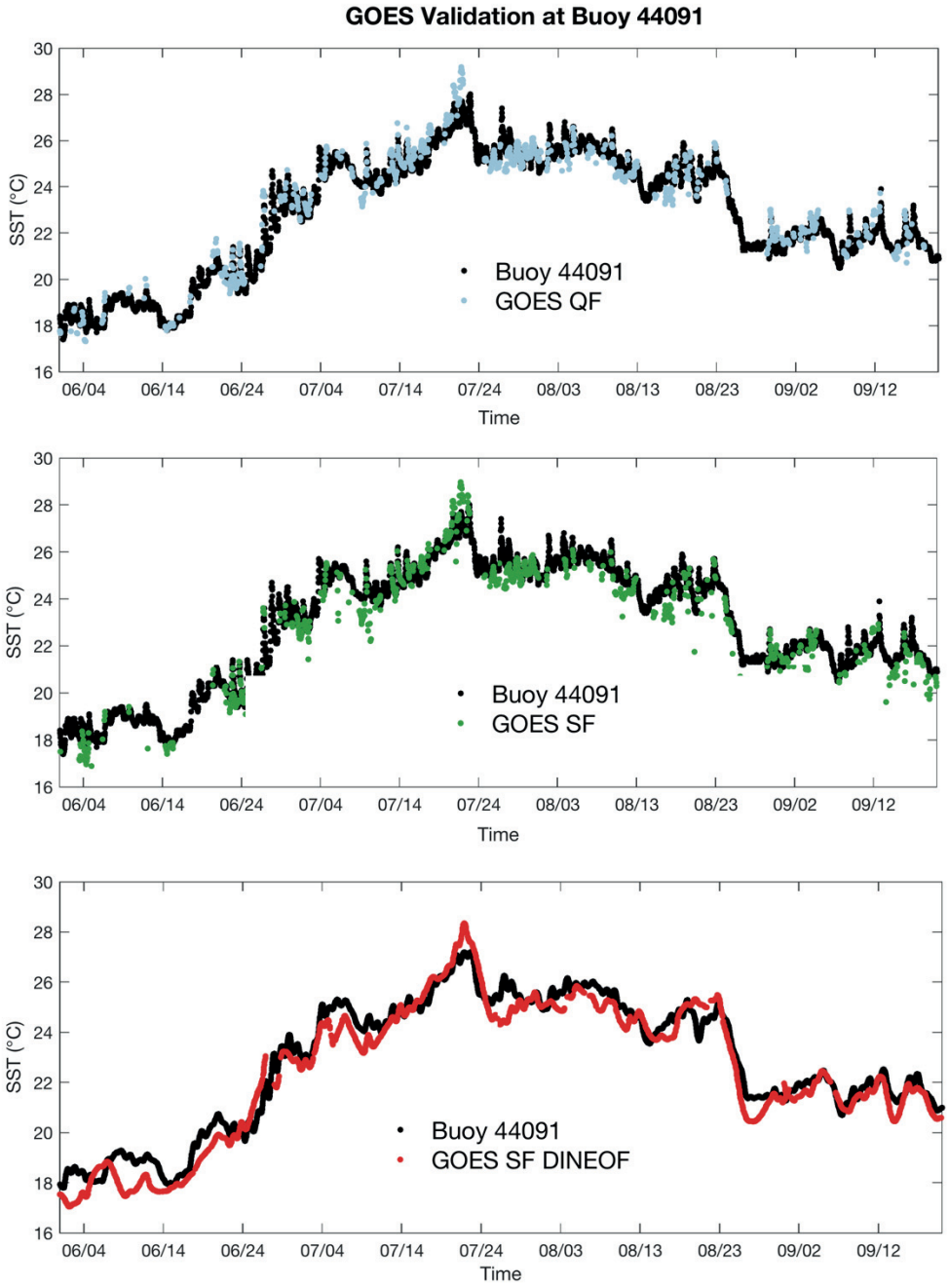

Figure 7. Validation of GOES SST data sets at Buoy 44091. GOES SST (colored dots): QF (Top), SF (Middle) and DINEOF (Bottom); and Buoy 44091 SST (black dots) are shown. GOES SF DINEOF is validated against a 24-hour smoothed buoy SST.

Sufficient SST coverage in the upwelling zone is important to ensure the accuracy of the DINEOF reconstruction. DINEOF reconstruction of GOES SF SST provided a complete hourly SST data set for the MAB 2019 summer. DINEOF is an EOF based technique that was used in this study to fill in missing SST data likely caused by the presence of clouds. The use of the 24-hour filter and the smoothing function allowed for the upwelling signal to be retained while remaining cloud edges were reduced (Alvera-Azcárte et al. 2009). Despite the gaps in GOES SF SST data, the DINEOF reconstructed GOES SST is accurate to buoy 44009 (Figure 7, Table 3). For example, around August 23, GOES SF DINEOF SST closely matches the SST observed at buoy 44091 despite a lack of GOES SF SST data at this location and time. GOES SF DINEOF SST contains 2315 measurements at each pixel which more than doubles the number of GOES SF measurements.

Table 3. Summary of SST validation statistics. Validation performed at NBDC buoys 44009, 44091, and 44065 for GOES QF, GOES SF, GOES SF DINEOF, AVHRR, and MUR. The GOES SF DINEOF SST is validated to a 24-hour smoothed buoy SST. Root Mean Square (RMS), Centered Root Mean Square (CMS), Model Bias (MB), and Count are calculated.

	BUOY	GOES QF	GOES SF	GOES SF DINEOF	AVHRR	MUR
RMS	44091	0.446	0.585	0.63	1.37	0.447
	44009	0.802	0.506	0.995	1.8	1.124
	44065	0.89	0.845	0.7086	1.42	0.675
CRMS	44091	0.441	0.535	0.56	1.26	0.445
	44009	0.716	0.499	0.985	1.72	0.943
	44065	0.8	0.845	0.7027	1.38	0.62
MB	44091	0.065	-0.237	-0.295	-0.54	0.047
	44009	0.37	0.083	-0.141	-0.53	0.611
	44065	0.39	-0.012	-0.092	-0.38	0.267
Count	44091	805	812	2314	135	111
	44009	737	843	2314	135	111
	44065	681	735	2315	122	111

2.4.3 Detecting Upwelling

Coastal upwelling was determined by a 2°C or more difference between inshore and offshore SST, as defined by Glenn et al. (2004). The inshore SST was extracted at the location of 4 recurrent upwelling centers and the offshore SST was extracted at a mid-shelf location, as indicated by the colored circles in Figure 3. Events were characterized by the persistence or lack of a 2°C or colder coastal SST for a minimum of 24 hours. The detection of upwelling is only compared between GOES SF DINEOF and MUR SST because they are both gap-filled datasets. In addition, SST data from GHRSST L3C AVHRR was infrequent at the 4 upwelling centers and contained corrupted cloudy data, so it was not useful for comparisons using this threshold.

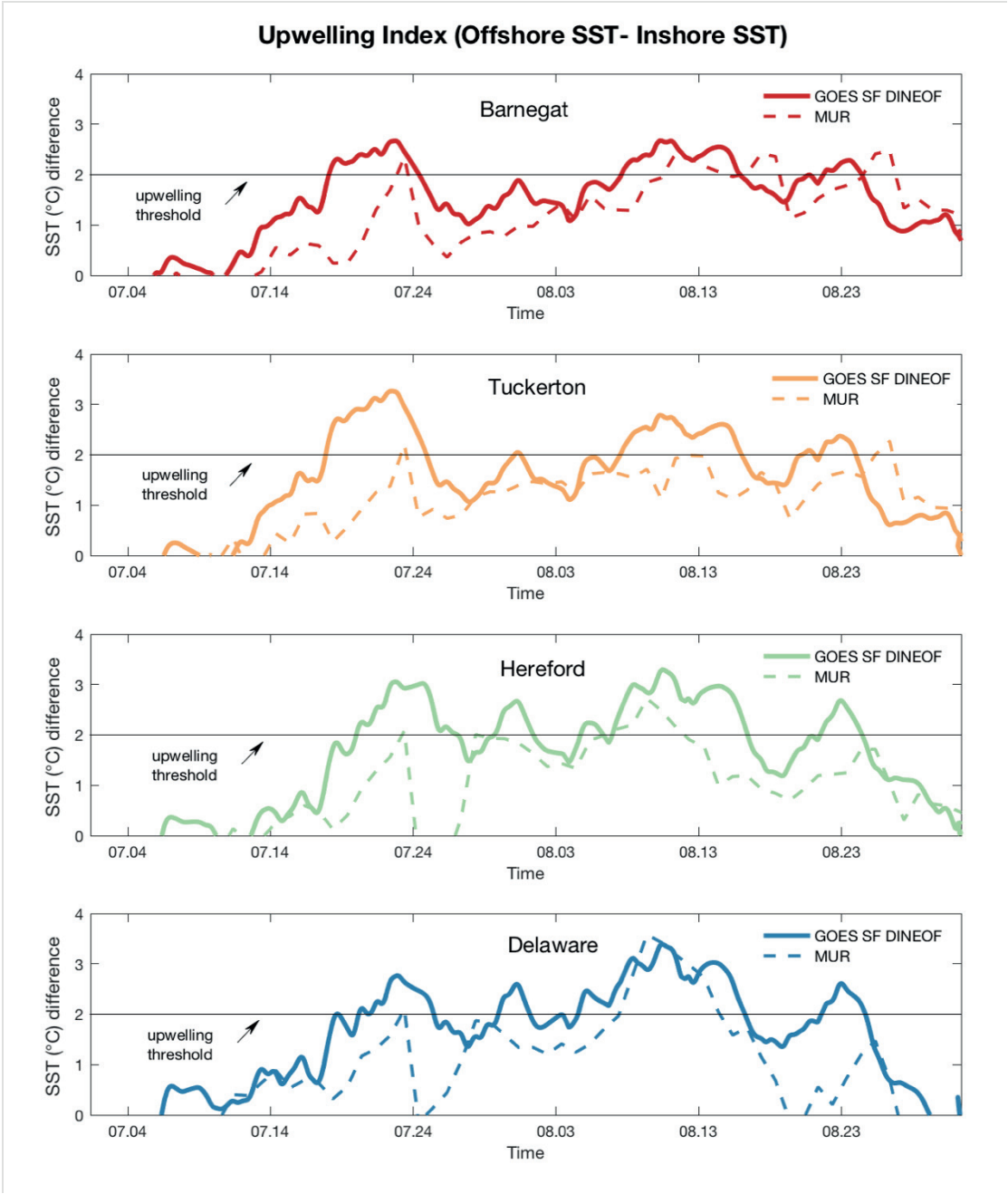

Figure 8. SST difference (offshore SST – inshore SST) at the 4 upwelling centers in the MAB for the summer time period. GOES SF DINEOF SST (solid lines) and GHRSST MUR SST (dashed lines) are shown. The upwelling threshold is defined as an SST difference in 2°C or greater.

Table 4. Upwelling detection results from GOES SF DINEOF and MUR for June 1- September 20, 2019. Results calculated for the days detected as upwelling by each product- GOES SF DINEOF (33 days) and MUR (15 days).

	GOES SF DINEOF	MUR
Total Upwelling Days	33	15
Percent of summer upwelling occurred (June 1- Sept. 20)	30%	13.5%
Average upwelling SST	22.5°C	22.97°C
Minimum upwelling SST	17.1 °C	17.88°C
Maximum SST Diff (Off-Inshore)	3.4 °C	3.58°C
Average Duration	6.5 days	3 days
Max Duration	17.66 days	7 days
Average Area Upwelling	3223 km^2	3091 km^2
Max Extent Area	5996 km^2	5799 km^2

During the upwelling season studied, June 1- September 20th, three upwelling events were detected in GOES SF DINEOF SST between July 17th and August 24th, 2019, totaling 33 days or roughly 30% of the summer (Figure 8, Table 4). The average duration of an upwelling event was 6.5 days and the longest event persisted for 17.66 days. Only 15 total days of upwelling were detected via MUR SST, with an average duration of 3 days and the longest event lasting 7 days. Winds at buoy 44009 were categorized as upwelling winds 18 hours earlier than the SST indicated upwelling, accounting for the local lag between wind and Ekman transport (Figure 9). The

occurrence of upwelling events detected via GOES SF DINEOF is physically confirmed by the presence of persistent, upwelling-favorable winds, primarily from the southwest. Winds that occurred during non-upwelling times appeared to be distributed across different directions.

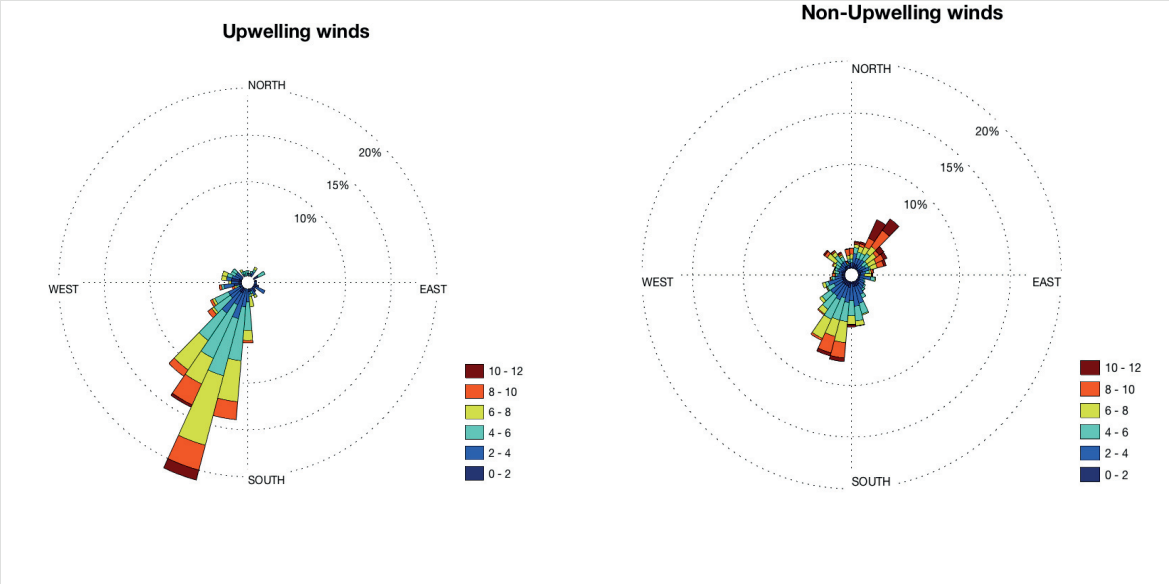

Figure 9. Winds at buoy 44009 during GOES SF DINEOF detected upwelling (left) and non-upwelling (right) times for the summer-time period. Wind speed (m/s) and direction (from) are shown. The winds are shifted 18 hours earlier than the timing of the upwelling events to account for the local lag in Ekman transport.

The average inshore upwelling SST at the 4 upwelling centers observed by both GOES SF DINEOF and MUR was ~22.7°C and the minimum upwelling SST was ~17.5°C. Only half of the days of upwelling detected by GOES SF DINEOF were detected via MUR. Figure 10 shows the median SST of each pixel averaged over the total upwelling events observed by GOES SF DINEOF and MUR. The median upwelling SST for GOES SF DINEOF contained colder SST pixels closest to shore, ~22°C, that are not present in MUR. In addition to the increased number of upwelling observations, GOES SF DINEOF provided more upwelling pixels per event, measured as the total

number of SST pixels above the upwelling threshold per SST image and indicated by the larger total area of upwelling (Figure 11). GOES SF DINEOF provided a detailed account of the spatial extent of upwelling with a maximum upwelling area of 4,410.9 km^2, the maximum area of upwelling observed via MUR was 3,128.3 km^2. Because MUR is a blended product that provides full spatial coverage of the MAB, the difference in upwelling area per event was not due to missing data.

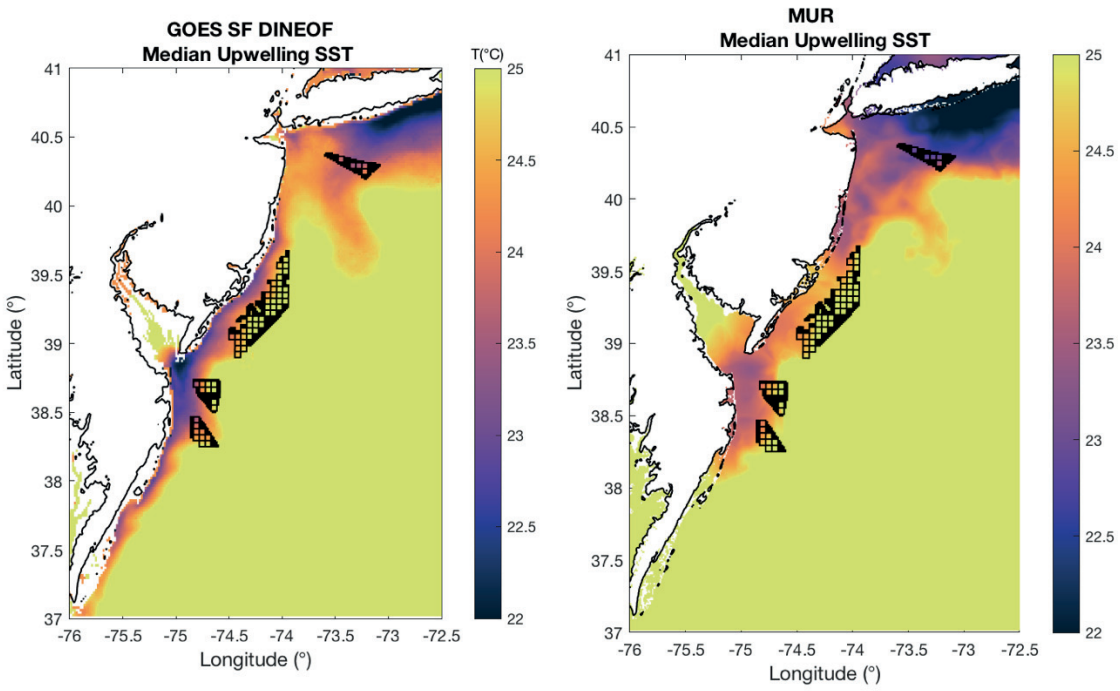

Figure 10. The median upwelling SST averaged per pixel for the detected upwelling days for GOES SF DINEOF (33 days) AND MUR (15 days). The black shaded polygons illustrate the offshore wind lease areas.

Without coastal SST from satellites during upwelling events, MUR is prone to estimating warmer SST in this area, causing fewer days to exceed the upwelling threshold. MUR generally agrees with GOES SF DINEOF in the timing of changes in the inshore-offshore SST difference for the four upwelling centers, but underestimates the

magnitude of this difference (Figure 8) and contains more spatially uniform, and warmer upwelling centers (Figure 10). When upwelling is detected by MUR, MUR and GOES SF DINEOF agree on the total area of upwelling (Figure 11), reinforcing the accuracy of the GOES Spike Filter and DINEOF reconstruction methods. However, for more than half of the time upwelling is detected by GOES, MUR estimates the area of upwelling to be close to zero, suggesting that retaining upwelling SST pixels via the Spike Filter method is helpful in improving the accuracy of GOES SF DINEOF reconstruction.

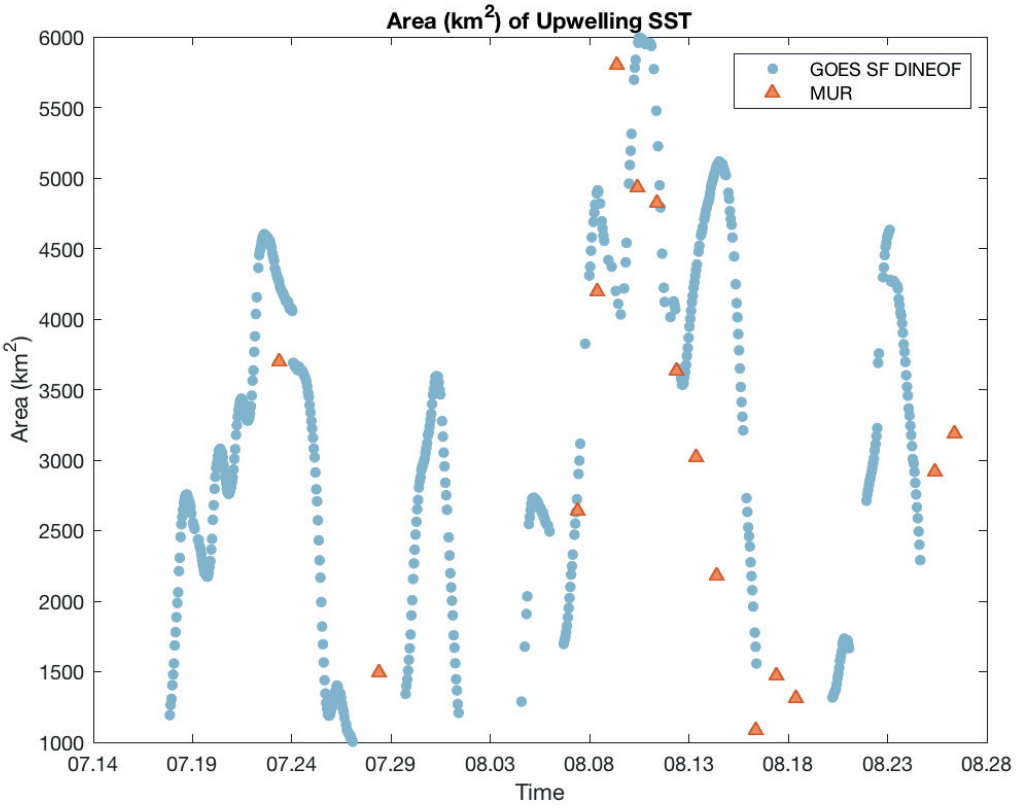

Figure 11. The total area (km2) of upwelling SST pixels as detected by GOES SF DINEOF (blue) and MUR (orange) during the upwelling time period.

2.5 Discussion

Coastal upwelling is a regional ocean phenomenon that is ecologically and physically important to the MAB. Given the dynamic nature of upwelling and the limitations to

satellite derived SST, the methods introduced in this study provide novel insight into the spatial and temporal evolution of upwelling events. Upwelling has been observed in the Mid Atlantic Bight in previous studies (Glenn et al. 2004; Seroka et al. 2018; Kohut et al. 2004) using AVHRR SST which provides less continuous viewing at equivalent or lower spatial resolution compared to GOES-16. Due to the lower temporal resolution of AVHRR, the presence of clouds can cause large gaps in time between available SST from AVHRR. These gaps in measurements make accurate characterization of the duration of upwelling events difficult.

The total number of upwelling days observed using GOES SF DINEOF in this study falls within the average range previously observed by a study of upwelling in the region using AVHRR (Glenn et al. 2004). However, the longest upwelling event observed in this study using GOES SF DINEOF is longer than the maximum outlier observed over 9 years of AVHRR measurements. In Glenn et al. (2004), the average observed lifetime of an upwelling event was ~1 week, and the largest outlier lasted approximately 2 weeks. In this study, the longest upwelling event persisted for over 17 days. The number of events observed in this study, ~3, is also on the lower range of the number of events per summer previously observed (3-8). This suggests that upwelling may be occurring more persistently, rather than a series of short episodic events as previously thought, due to improved detection via a more continuous SST data set.

Coastal upwelling events that were both wind-driven and influenced by tidal mixing were observed in this study along the New Jersey coast and the Delaware Bay. Southerly winds are predominant in the summertime, a driver of coastal upwelling along the New Jersey shelf (Kohut et al. 2004) and consistent with the timing of upwelling

events observed during this study. The onset and termination of upwelling events detected using GOES SF DINEOF were more distinct and separated by non-upwelling for longer at the two northern upwelling centers (Barnegat and Tuckerton), while upwelling persisted longer at the two southern sites (Hereford and Delaware). For example, the largest upwelling events persisted for 17.66 days at Hereford and for 11 days at Delaware during the first half of August, while the longest upwelling event at Barnegat and Tuckerton occurred earlier in the season around mid-July. In the beginning of the summer season, notably for the first upwelling event, coastal SST is ~1°C colder at the two northern sites. Heading into late July/early August, coastal SST was slightly colder at the two southern sites by ~0.5 – 1°C, possibly due to the seasonal evolution of the Cold Pool which is the source of the upwelled water; the Cold Pool warms at a rate of ~1°C/month but this rate varies and is stronger over Georges Bank and the New York Bight than it is in the southern Mid Atlantic Bight (Lentz 2017). In addition, the longer persistence of upwelling events in Delaware Bay is consistent with previous observations and may be influenced by tidal mixing (Voynova et al. 2013). Münchow et al. (1992) suggested that near the Delaware Bay, tidal currents are strong and likely enhance and extend the presence of cold water from upwelling. Voynova et al. (2013), also describe the presence of a shallow canyon (30-40m) that may allow for a more pronounced Ekman spiral to develop.

Another limitation to satellite SST products is that quality filtering algorithms frequently characterize cold coastal upwelling SST as corrupted data. While an algorithm has been developed to retain upwelling pixels for AVHRR SST in the MAB (Glenn et al. 2016), this algorithm is locally focused with region-specific thresholds, and dependent on

channels that are not provided by all sensors. Therefore, this algorithm has not yet been applied to GOES SST and is not applied to global products like GHRSST L3C AVHRR or MUR SST. The Spike Filter method developed in this study for GOES is also specific to the ocean conditions of the MAB and is not a global solution. The Spike Filter is rudimentary and more permissive than the quality filter developed for GOES and may allow for the presence of corrupted cloudy pixels. In addition, the methods used in this study are limited in that they cannot be applied instantaneously. SST from GHRSST L3C AVHRR at the 4 upwelling centers was infrequent and contained corrupted cloudy data, so it was not useful for the characterization of upwelling events using the SST difference threshold. Due to the quality filtering applied to satellite SST products, it is likely that near-coast upwelling SST pixels are not assimilated into the MUR product. Less than half the number of total upwelling days observed using GOES SF DINEOF were observed in MUR SST. The link between upwelling and the MAB ecology is well documented, and accurate detection of the upwelling occurrence is important for ocean and atmospheric modeling as well as for fisheries operations and management in the Mid Atlantic.

Coastal upwelling has also been shown to impact the offshore component of sea breeze circulation (Seroka et al. 2018), the timing of which is critical to the offshore wind industry. Offshore wind operations will rely on accurate wind forecasting to match electricity demands. Filaments of upwelling were observed to extend entirely through portions of the NJ wind energy area and were present in the shoreward half during most of the upwelling events. The location of the current wind energy areas in the MAB are shown in Figure 10 as shaded polygons. Upwelling SST frequently occupied the entirety

of the offshore wind leased areas off Delaware and Long Island. Seroka et al. 2018, simulated the impacts of upwelling on sea breeze circulation using a maximum averaged upwelling SST from AVHRR imagery. As demonstrated in this study, upwelling events are extremely dynamic and may be occurring more frequent, and for longer durations than can be detected by lower resolution products like AVHRR and MUR. Using high resolution GOES SST as atmospheric modeling input may provide further insight into the effects of upwelling on sea breezes in the Mid Atlantic.

2.6 Conclusion

This study demonstrates the value of GOES hourly SST in improving observations of coastal upwelling in the Mid Atlantic Bight. When compared to global SST products like AVHRR and MUR, GOES provides 2000 additional SST measurements at regional buoy locations over the peak upwelling season and detects more than twice the amount of upwelling days. The default GOES quality filter frequently removes cold upwelling pixels which has been previously identified as a problem for quality filtering in many satellite SST sources. We developed a method that retained coastal upwelling SST data that was likely not included in AVHRR or the MUR SST composite, and was effective in maintaining the accuracy of GOES SST. This method allowed for a more accurate reconstruction of GOES inshore SST. This study demonstrates the importance of developing an operational quality filtering algorithm for GOES SST that retains upwelling pixels so that it can be readily used to improve observations of coastal upwelling in the Mid Atlantic Bight. An improved bias correction technique should also be developed that can be applied to upwelling retained in GOES SST.

Coastal upwelling is a unique feature that must be accurately represented in terms of temperature, frequency, and duration because of its importance to the ecology and physics of the region. Previous studies have used AVHRR imagery which has lower temporal resolution and can be significantly obscured by clouds. The use of GOES hourly SST to observe upwelling has suggested that upwelling events may be more persistent than previously thought. Future climatology studies of upwelling in the MAB should use cloud-free upwelling retained hourly GOES SST to accurately characterize the temporal and spatial evolution of coastal upwelling and the unique physical conditions of the Mid Atlantic Bight. Improvements to the characterization of upwelling are especially useful to the fishing and renewable energy industries. Upwelling events have been linked with hypoxic bottom conditions off the NJ coast (Glenn et al. 2004) and delivery of subsurface nutrients that support phytoplankton primary production to the lower Delaware Bay (Voynova et al. 2013). Upwelling has also been shown to influence sea breeze circulation and is a research interest of the offshore wind industry (Seroka et al, 2018). Atmospheric modeling studies should be conducted using hourly updating GOES SST to provide realistic ocean conditions and determine the impact of SST fields on wind forecasting.

Chapter 3

Sensitivity of RU-WRF winds to SSTs during Coastal Upwelling

3.1 Introduction

Sea Surface Temperature (SST) is a critical parameter in oceanographic studies but is also important for weather forecasting and atmospheric modeling (NOAA 2020). SST is measured using temperature sensors on satellites, buoys, ships, and other methods. SST provides insight into interactions between the ocean and atmosphere which are constantly exchanging heat, water, and momentum (Xie 2018). Oceans absorb solar radiation, a source of energy for motion, making SST important for atmospheric temperature conditions and circulation. For example, surface winds affect ocean surface heat flux and drive ocean currents. SST also regulates atmospheric convection which also modulates ocean conditions. For example, SST is important for identifying El Niño and La Niña cycles. On a more local scale, SST is important in understanding sea-breeze circulation in coastal regions (Seroka et al. 2018; Franchito et al. 1998).

Numerous studies have demonstrated the importance of SST in modeling (DeMott et al. 2016; O'Neill, Chelton, & Esbensen 2010; Song et al. 2004; Chelton 2005). One study highlights the inability of global models to simulate the Madden-Julian Oscillation (MJO) accurately due to variations in SST (DeMott et al. 2016). They illustrated the importance of accurate measurements rather than relying on static models to get an authentic understanding of the system. On broad spatial scales, spanning ocean basins, perturbations in SST are found to be negatively correlated with wind speed perturbations as large-scale atmospheric circulation patterns change surface ocean temperatures

through modulation of surface heat fluxes and upper ocean mixing (O'Neill, Chelton, & Esbensen 2010). On a synoptic scale (100-1000km), surface wind speed and SST perturbations are positively correlated. The use of high-resolution SSTs in a mesoscale model in Song et al. (2004) produced a realistic simulation of the marine atmospheric boundary layer (MABL). Chelton (2005) demonstrated the sensitivity of the MABL in a weather forecasting system to the underlying SST and also that data forecasts using higher-resolution SST compared more favorably to near-surface wind stress. However, Lombardo et al. (2018) found that fine-scale SST may be beneficial in less stable sub-tropical environments but may not produce more accurate sea-breeze simulations in highly stable MABL regimes. They found that in highly stable MABL regimes, the largest thermal perturbations were confined to the lowest 10% of the seabreeze column.

Satellite SST is limited in that it is often obscured by clouds, making the accurate characterization of dynamic ocean events, like coastal upwelling, difficult. In addition, many quality filtering algorithms are designed to work on a global scale and are not calibrated to the SSTs of local events. For example, it has been shown that the quality algorithm for global GOES and AVHRR and MUR SST products remove coastal upwelling pixels as they are flagged as corrupted or bad pixels. Therefore, it is important that high temporal and spatial resolution SST and locally focused quality control methods are applied to SSTs for use in modeling and forecasting of focused areas.

The stratification of the Mid-Atlantic Bight varies greatly by season. During the winter and early spring, the ocean across the entire shelf is well mixed and cold (Bigelow 1933). During the summer, the MAB is a highly stratified ocean with warm surface waters and remaining winter water on the bottom, known as the Cold Pool (Houghton et

al. 1982). The summertime is also when coastal upwelling events occur, driven by southerly winds. Due to the Bermuda High, seasonal synoptic winds flow from the southwest and drive Ekman transport of surface ocean water offshore. The cold remnant winter water is then driven up along the coast, dropping sea surface temperatures 2-8° C (Glenn et al. 2004).

Coastal upwelling creates a higher thermal contrast between the warm land and cold ocean surface and has been shown to influence sea breeze fronts (Franchito et al. 1998; Seroka et al. 2018). Surface wind blows from the colder ocean to the warmer land and at a higher altitude and the return flow blows from land to sea. Franchito et al. (1998) showed that in the Brazilian coastal region, most of which is influenced by the sea-breeze circulation, coastal upwelling intensified the ocean-atmospheric processes. Local winds influence the characteristic air flow, precipitation, humidity, and pollutant transports (Franchito et al. 1988). During a simulated upwelling event in the MAB, the sea breeze began earlier and was more intense (Seroka et al. 2018). Because of the anticipated development of offshore wind energy and the ocean-atmospheric interactions during coastal upwelling events, the MAB is an ideal area to test the sensitivity of wind forecasting to SST fields.

Offshore wind is a variable source of electricity, bringing challenges for integration into the electric grid. The electric grid requires power system and market planning and management to balance the supply and demands of the system (Foley, Leahy, & Mckeogh 2010). Wind power forecasting is used by system operators so that they can plan the amount of electricity that will be supplied to the grid and by wind developers to maximize profits. Wind resource assessment is also critical in the

development, siting and operation of a wind farm. Improving the forecasting and measurement of wind speed and direction allows for the production of offshore wind energy at a lower cost to consumers (DOE 2016). In the MAB, complex metocean dynamics like strong coastal upwelling and storm mixing have been shown to influence wind conditions at turbine hub heights (Optis et al. 2020). Coastal upwelling events occur for up to half of the days of the summer in the MAB (Glenn et al. 2004) and coincide with peak summer energy demands (Seroka et al. 2018). Previous studies have shown the importance of upwelling in influencing sea-breeze circulation in the MAB (Seroka et al. 2018). However, there have not been studies using realistic ocean SSTs at a high spatial and temporal resolution for wind forecasting in the MAB offshore wind energy areas.

This study is aimed at preforming a sensitivity test of WRF wind speeds at hub height in a NJ offshore lease area to varying spatial and temporal resolution SSTs. This case study will also test the sensitivity of regionally focused cloud correcting on SSTs during an upwelling event. In this section we will use three different ocean surface boundary conditions and complete three RU-WRF runs for 7/15/19-7/23/19 during a coastal upwelling event. The forecasted wind speeds from each of the three RU-WRF runs will be compared at a location in the NJ WEA. This section is organized as follows. Section 3.2 presents the details of the RU-WRF model and the ocean surface boundary conditions chosen for each of the three RU-WRF runs. In Section 3.3, RU-WRF SST is examined and forecasted wind speeds are compared and converted to wind power production. Section 3.4 includes a summary of the results and guidance for future analyses.

3.2 Methods

The Weather Research and Forecasting mesoscale model (RU-WRF) is operated by the Rutgers University Center for Ocean Observing Leadership and is centered over New Jersey and the Mid-Atlantic Bight. This model runs a parent nest at 9km resolution and a child nest at 3km resolution. The 3-km domain spans the coastal region from southern Massachusetts to North Carolina. The geospatial coverage includes an altitude of 30.0m to 250.0m at a resolution of 10.0m. The real-time model is run daily following the 00Z cycle of the Global Forecast System (GFS) and utilizes a cold-pixel SST reconstruction from AVHRR. The coldest pixel SST product uses a declouding and compositing method that is regionally focused to retain coastal upwelling pixels that are often removed using global quality control methods. RU-WRF was evaluated by the National Renewable Energy Laboratory (NREL) for its atmospheric observation and modeling capabilities for characterizing the NJ offshore wind resource (Optis et al. 2020). NREL found that the coldest pixel product was more accurate compared to other widely used SST products in the region and helped to improve model accuracy (Optis et al. 2020).

The first run, GFS, is the default version of WRF and contains a lower resolution global SST product than AVHRR coldest pixel. The second run of this study, AVHRR coldest-pixel, represents an example of the operational mode of RU-WRF which is locally cloud corrected for upwelling and is at a high spatial resolution. The third run, GOES SF DINEOF, provides SSTs at a similar spatial resolution to the current AVHRR coldest pixel product but has a higher temporal resolution and is statistically gap-filled (See section 2.3 for details). The GOES SF DINEOF SST may provide a higher level of detail than what is provided by the operational AVHRR coldest pixel SST product.

This case study includes three RU-WRF 4.1 runs for 7/15/19-7/23/19 using the 3km processed, best datasets for analyses. The processed data is extracted from the raw WRF output to include only the variables that are needed and is extrapolated to defined and regular heights (every 10m from 10m-250m). The best dataset is a continuous time series containing only the first 24 hours out of each model run pieced together. Each model run is 48 hours long so the second 24 hours of each model run is replaced with the most recent 24 hours so that the best data set contains the most accurate forecast. This week was chosen because of the occurrence of upwelling off of New Jersey coinciding with high air temperatures (>32°C) and peak energy demand. In addition, a corkscrew and pure seabreeze was detected throughout the majority of this week. The three runs included 3 different SSTs as the ocean surface boundary condition: 1. GFS 2. AVHRR coldest-pixel and 3. GOES SF DINEOF.

1. GFS: The Global Forecasting System (GFS) 0.25◦×0.25◦ forecast data product initialized at 00:00 Universal Time Coordinated (UTC). The GFS forecasting product is produced by the National Center for Environmental Prediction https://www.nco.ncep.noaa.gov/pmb/products/gfs and is provided every 6 hours as the default SST product to RU-WRF. This is a data assimilative product which includes analyzing SSTs from both satellite radiances and in situ sea water temperatures and extending them to Near-Surface Sea Temperature (NSST) temperature profiles (Li et al. 2018). No additional SST data is provided for this model run. The results from this model run can be accessed here: http://tds.marine.rutgers.edu/thredds/dodsC/cool/ruwrf/wrf_gfs_4_1_3km_processed/WRF_GFS-only_4.1_3km_Processed_Dataset_Best

2. AVHRR coldest-pixel: The coldest-pixel product uses satellite observations from the Advanced Very High Resolution Radiometer (AVHRR). This product is a custom feature of the operational RU-WRF model runs and is designed to capture more cold upwelling events. The coldest-pixel daily composite can be accessed here: http://tds.maracoos.org/thredds/dodsC/Rutgers-Coldest-Pixel-Agg.nc. The coldest-pixel SST is provided as a three-day composite with the most recent daily composite stacked on top at approximately .02◦×.02◦ spatial resolution. In cases where data is not available Short-term Prediction Research and Transition Center (SPoRT) SST data product is used to fill data gaps. The results from this model run can be accessed here: http://tds.marine.rutgers.edu/thredds/dodsC/cool/ruwrf/wrf_4_1_3km_processed/WRF_4.1_3km_Processed_Dataset_Best
3. GOES SF DINEOF: (see Chapter 2 for details). This data originates from the GOES-16 satellite which takes images at 15-minute intervals at approximately .02◦×.02◦ spatial resolution and can be accessed at https://podaac.jpl.nasa.gov/. The hourly composited data was cloud-corrected to retain upwelling and gap-filled using DINEOF. The SST is ingested as 3-hour composited images in RU-WRF. GFS SST is filled in outside of the 3km RU-WRF domain. The results from this model run can be accessed here: http://tds.marine.rutgers.edu/thredds/dodsC/cool/ruwrf/wrf_goes_4_1_3km_processed/WRF_GOES_DINEOF_SST_4.1_3km_Processed_Dataset_Best

3.3 Results and Discussion

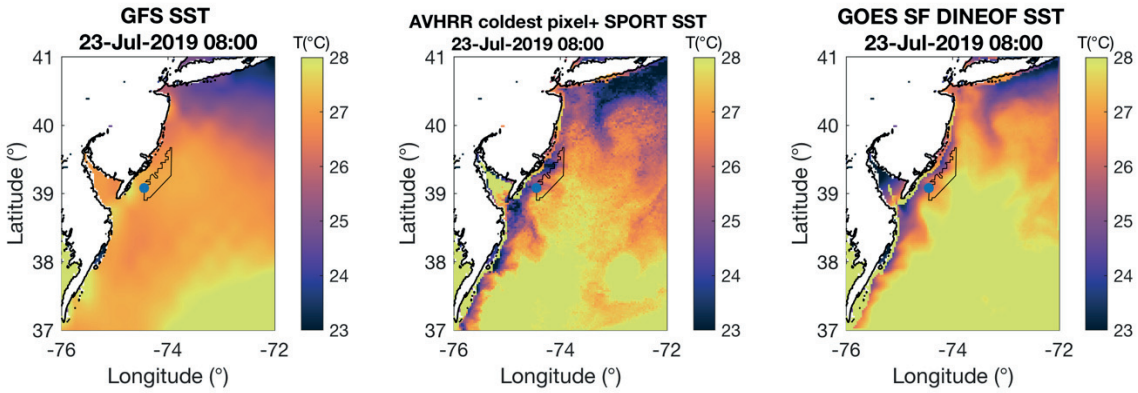

Figure 12. RU-WRF SST image on July 23 8:00 UTC provided by GFS, AVHRR Coldest pixel + SPORT, and GOES SF DINEOF. The location of Ocean Wind 1 Buoy (OCW1) is indicated with a blue circle and the NJ wind energy area (WEA) is outlined in black.

Upwelling off NJ and DE is captured well by AVHRR coldest pixel and GOES SF DINEOF SST and is completely absent from GFS SST. The first upwelling event in the summer of 2019 occurred from July 17th through July 31st. The upwelled coastal SST was ~3-5°C colder than offshore SST. AVHRR SST is coarser in resolution than GOES SF DINEOF but the spatial and temporal extent of upwelling detected is very similar. The mid-shelf GFS SST is about 2°C colder than the SST detected by AVHRR and GOES SF DINEOF satellites for most of the time period studied. There was rapid warming of the offshore SST during this time period that was not captured by GFS SST.

Upon review of the SST images, cold speckled SST pixels were present on some AVHRR coldest pixels images, suggesting the presence of cloudy data. The coldest pixel images also appear coarser with artifacts possibly being introduced through the compositing and gap filling methods. In addition, there is thin strip of warmer SST along

the coast in AVHRR coldest pixel and GOES SF DINEOF that is likely where data is missing and is being filled in with GFS SST by WRF. This study highlights the need for further investigation of the SST products being used in RU-WRF analyses as SST is critical to the air-sea energy exchange and forecasted winds offshore.

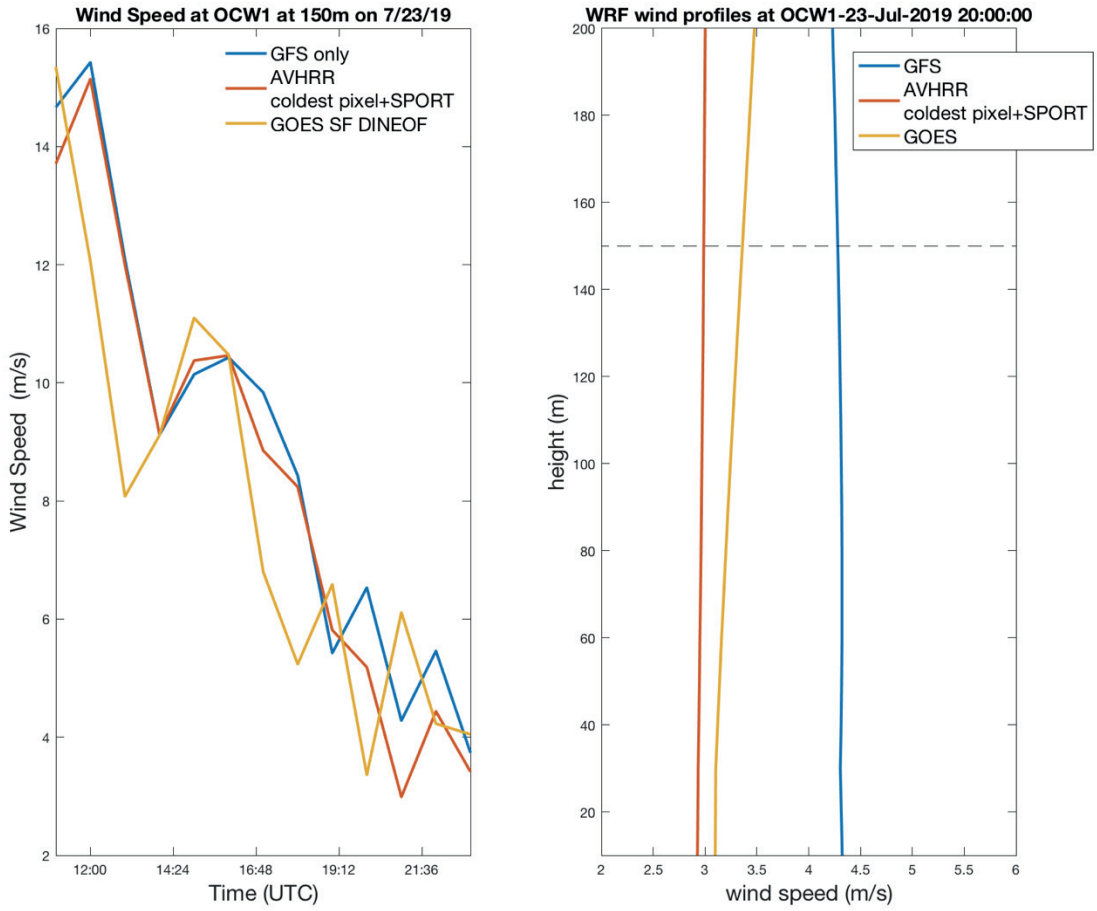

Figure 13. Wind speeds on 7/23/19 at OCW1 from RU-WRF using three different ocean surface boundary conditions. On the left are wind speeds at hub height (150m) and on the right is a profile of the wind speeds from 10-200m at 20:00 UTC.

Wind speeds were extracted at the location of OCW1 (longitude –74.17791° and latitude 39.13419°) Figure 13. This is an example of when there was a difference in wind speeds between the three different RU-WRF runs. On the left is the wind speeds on 7/23/19 extracted at 150m which is the hub height for a 15MW turbine. There appears to

be a difference in the timing of changes in wind speeds. For example, RU-WRF using AVHRR coldest pixel and GFS predicts high wind speeds until 13:12 UTC whereas GOES SF DINEOF predicts a drop in wind speeds an hour earlier. Again, RU-WRF using GOES SF DINEOF predicts changes in wind speeds about an hour earlier than RU-WRF using GFS between 18:00 to 22:48 UTC. The timing of the changes in wind speeds agree between the GFS and AVHRR coldest pixel RU-WRF runs on this day. However, toward the end of the day, the AVHRR coldest pixel run contains lower wind speeds (~3 m/s), which is more consistent with the GOES SF DINEOF run, than the GFS run (~5 m/s)

On the right is a profile of the wind speeds from 10-200m at 20:00 UTC for all three RU-WRF runs. This time was chosen as an example of a time where the wind speeds were different at 150m. The wind profiles for all three runs on this day were fairly uniform between 30-200m. This demonstrates that the difference in wind speed is consistent at these heights for each WRF run.

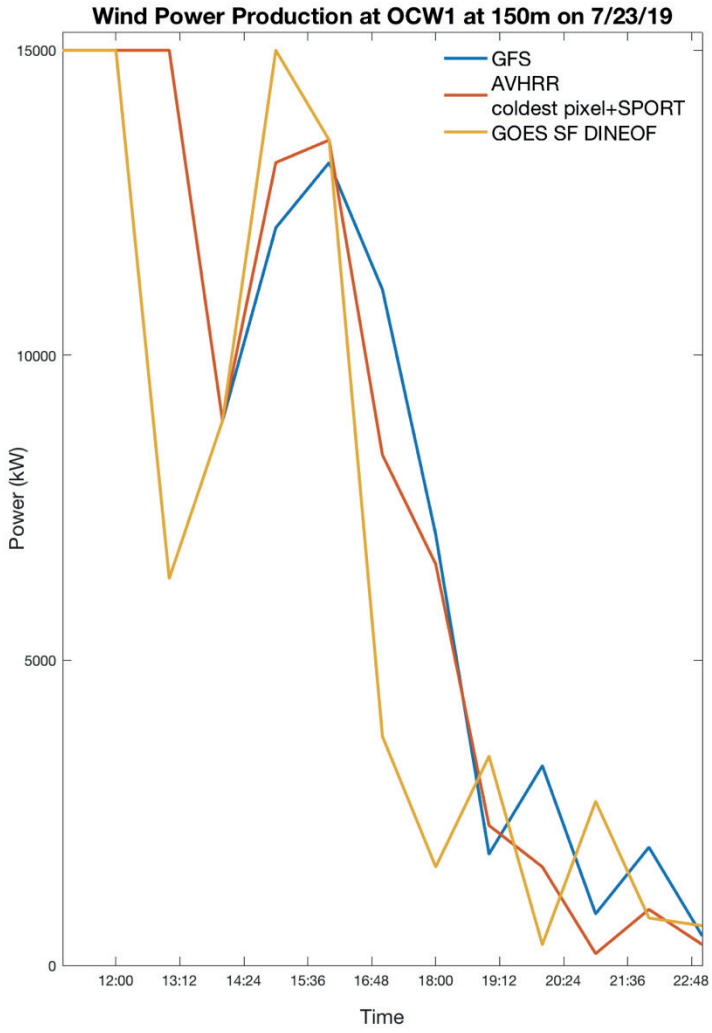

Figure 14. Wind Power Production on 7/23/19 based on RU-WRF wind speeds at OCW1 at 150m using three different ocean surface boundary conditions.

Wind speeds were extracted from each RU-WRF run at 150m at the location of OCW1 and were then converted to power using the power curve for the IEA 15MW turbine (Gaertner et al. 2020) (Figure 14). This turbine has a hub height of 150m, a cut-in speed of 3 m/s, a cut-out speed of 25 m/s, and rated speed of 10.84 m/s at which it can produce 15,000 kW. There is a noticeable difference in the amount and timing of power

that could be produced by a wind turbine located OCW1 on this day based on RU-WRF predicted wind speeds using the three different ocean boundary conditions. For example, around 17:00 UTC, this difference is as large as 9,000kW. On this day, from 12:00 to 21:36 power production changed from a maximum amount for a 15MW turbine to very low amounts, demonstrating the importance of accurate wind forecasting in order to meet grid demands.

Table 5. Wind Power Production on 7/23/19 based on RU-WRF wind speeds at OCW1 at 150m using three different ocean surface boundary conditions.

SST input	Total GWh	Capacity Factor
GFS	1.3023	0.4201
AVHRR Coldest-pixel+ SPORT	1.3786	0.437
GOES	1.2691	0.409

The total energy production in GWh was calculated as a sum of the instantaneous power output corresponding to each hourly forecasted wind speed at OCW1 throughout the entire case study (7/15/19-7/23/19). The capacity factor is a ratio of the total energy production to the maximum possible energy production for the total time period. The maximum difference in total energy production between the 3 RU-WRF runs is 90,400 kWh (Table 5). This difference in energy production is equivalent to a difference in energy consumption by ~414 households, based on the average per household energy consumption in New Jersey (EIA 2009). The capacity factor ranged from .409 to .437 which means that from 7/15/19-7/23/19 a 15MW turbine at OCW1 could have produced ~42% of its maximum capacity of wind energy.

3.3 Conclusion:

The purpose of this analysis was to test the sensitivity of RU-WRF forecasted winds to varying temporal and spatial resolution SSTs. This brief study demonstrated that when using different ocean surface boundary conditions in RU-WRF, there is a difference in forecasted wind speeds at hub height in the NJ WEA. For 715/19-7/23/19, there was a total maximum difference in power production at one 15MW turbine of 90,400 kWh based on the RU-WRF wind speeds at hub height for the three runs. In addition, there were differences in the timing of changes in wind speeds between the three models. This demonstrates the importance of SST as a parameter in atmospheric modeling.

Future studies should include a longer analysis of the impact of SST, such as a seasonal analysis, especially considering the potential of more persistent upwelling being captured by GOES SF DINEOF (see Chapter 2). In addition, increasing the temporal resolution of GOES SF DINEOF SST to hourly updating data would help to further investigate the impact of SST resolution on RU-WRF wind speed output. Upon evaluating RU-WRF, NREL recommended the use of an hourly data set that represented the diurnal evolution of SST (Optis et al. 2020). Therefore, GOES hourly SST may provide the opportunity to address this recommendation in order to improve simulation accuracy. This analysis did not address the atmospheric physics driving changes in wind speeds due to varying SST fields. Validation of SST and wind speeds could be completed with the newly available data from the Atlantic shores buoy for the following summer time period located in the NJ WEA or other relevant data sets.

The SST of the ocean is important as it provides insight into interactions between the ocean and atmosphere. The MAB is a unique oceanographic environment that contains dynamic events like coastal upwelling which can occur for half of the summer (Glenn et

al. 2004) and coincide with peak energy demands (Seroka et al. 2018). The PJM energy market procures energy demands in the day-ahead market and in real-time (5 minutes ahead). As New Jersey and the rest of the US prepares for the development of offshore wind, improving the accuracy of wind forecasting is an important tool in ensuring the efficient operation of the industry.

Chapter 4

Conclusions

The findings of this thesis demonstrate the importance of using newly available GOES SST and provide the motivation for adapting this product for oceanographic and atmospheric analyses. This product provides unique insight into the extent and evolution of coastal upwelling events in the MAB and can be valuable for improving our understanding of other regional phenomena. Coastal upwelling events are important to stakeholder groups like fisheries and offshore wind. Both stakeholder groups are reliant on accurate oceanographic data to operate efficiently. With a changing offshore environment, the fisheries industry will face new sets of challenges and will require improved monitoring and understanding of the ocean to adapt. Further insight into ocean-atmospheric interactions in the MAB will be invaluable to the offshore wind industry and will aid in optimizing the capture of renewable energy.

The main objective of this thesis is to investigate the detection of coastal upwelling in the MAB using newly available high resolution GOES-16 SST and to demonstrate the impact of this dataset on RU-WRF forecasted wind speeds. Various SST products were compared throughout this thesis for their ability to provide a realistic representation of the MAB for both oceanographic and atmospheric studies. The ability to observe our oceans has vastly increased with satellite technology and continues to improve with higher resolution imagery. The MAB is a unique oceanographic environment that requires advanced observational and modeling technology to accurately characterize and understand its dynamics. The Cold Pool, a key component of the MAB, is a cold-water mass that develops below the seasonal thermocline from remnant winter water and

remains present in the mid to outer shelf throughout the summer. The Cold Pool is the source for coastal upwelling, which is focused upon in this thesis as an example of a dynamic MAB feature that affects existing stakeholder groups. Coastal Upwelling was previously defined by Glenn et al. (2004) as a difference between onshore and offshore SST of at least 2°C. Using this definition, we can describe coastal upwelling events, both in size and duration from SST fields. Further analyses include the use of GOES SF DINEOF in RU-WRF, as the ocean surface boundary condition, amongst others, to highlight how SST impacts forecasted wind speeds offshore. The following in a summary of the conclusions of each chapter.

Chapter 2 demonstrates that hourly GOES-16 SST is valuable for the detection of coastal upwelling and highlighted the need for cloud-correcting methods that are regionally focused so that unique features like coastal upwelling are not flagged as corrupted pixels in the MAB. This chapter includes the methods that were developed to create a cloud-corrected gap-filled hourly high-resolution SST data set (GOES SF DINEOF) derived from the GOES-16 satellite for the summer of 2019. This method was validated and was effective in maintaining the accuracy of GOES SST while retaining more upwelling pixels. A major finding from using the GOES SF DINEOF SST data was that upwelling may be occurring more persistently than previously thought. In addition, GOES SF DINEOF SST detected more than double the number of upwelling days when compared to the global SST product MUR. This analysis demonstrated the value of regionally focused applications to global SST products in order to study dynamic events like coastal upwelling. This analysis also highlights the need for an operational cloud correction algorithm to be developed for GOES SST.

Chapter 3 presents a brief sensitivity test of RU-WRF to varying ocean surface boundary conditions. Three SST fields were chosen for RU-WRF with varying spatial and temporal resolution. The third run used the GOES SF DINEOF data from chapter 2, reduced to 3-hour composites, which represents a high spatial and temporal resolution SST with regionally focused cloud-correcting to build upon the operational SST product being used. The main finding of this case study was that the forecasted winds at hub height at a point in the NJ WEA were different in both timing and magnitude as a result of using the three different SST fields. This would also affect the ability for offshore wind to efficiently provide electricity to match grid demands. This analysis makes the case for a longer, more detailed study that includes validation data to determine which SST product may improve the accuracy of RU-WRF forecasted winds and what level of resolution is necessary.

Bibliography

Alvera-Azcárate, A., A. Barth, D. Sirjacobs, and J.M. Beckers, 2009: Enhancing temporal correlations in EOF expansions for the reconstruction of missing data using DINEOF. *Ocean Sci.*, **5**, 475-485.

Benway, R. L., and J. W. Jossi, 1998: Departures of 1996 temperatures and salinities in the Middle Atlantic Bight and Gulf of Maine from historical means. *Journal of Northwest Atlantic Fishery Science,* **24**, 61-86.

Bigelow, B., 1933: Studies of the waters on the continental shelf, Cape Cod to Chesapeake Bay. I. The cycle of temperature. *Physical Oceanography and Meteorology,* **2**, 135.

Bigelow, H. B., and W. C. Schroeder, 1953: Fishes of the Gulf of Maine. *Fisheries Bulletin,* **53**, 1-577.

Castelao, R., S. Glenn, and O. Schofield, 2010: Temperature, salinity, and density variability in the central Middle Atlantic Bight. *Journal of Geophysical Research: Oceans,* **115**, C10005.

Chapman, D. C., and R. C. Beardsley, 1989: On the origin of shelf water in the Middle Atlantic Bight. *Journal of Physical Oceanography,* **19**, 384-391.

Chelton, D. B., 2005: The impact of SST specification on ECMWF surface wind stress fields in the eastern tropical Pacific. *J. Climate*, **18**, 530–550.

Chen, Z., 2018: Dynamics and spatio-temporal variability of the Mid-Atlantic Bight Cold Pool. Ph.D. dissertation, Rutgers, The State University of New Jersey.

Chen, Z., and E. N. Curchitser, 2020: Interannual Variability of the Mid-Atlantic Bight Cold Pool. *Journal of geophysical research. Oceans,* **125**.

Chen, Z., E. Curchitser, R. Chant, and D. Kang, 2018: Seasonal Variability of the Cold Pool Over the Mid-Atlantic Bight Continental Shelf. *Journal of Geophysical Research: Oceans,* **123**, 8203-8226.

DeMott, C. A., J.J Benedict, N.P. Klingaman, S.J. Woolnough, and D.A.Randall, 2016: Diagnosing ocean feedbacks to the MJO: SST-modulated surface fluxes and the moist static energy budget. *J. Geophys. Res. Atmos.*, **121**, 8350– 8373.

DOE, 2016: Offshore Wind Technologies Market Report, https://www.energy.gov/eere/wind/downloads/2016-offshore-wind-technologies-market-report (Accessed June 12, 2020).EIA, 2009: Household Energy Use in New Jersey. Data from EIA's 2009 Residential Energy Consumption Survey., https://www.eia.gov/consumption/residential/ (Accessed November 20, 2020).

Fairbanks, R. G., 1982: The origin of continental shelf and slope water in the New York Bight and Gulf of Maine: evidence from $H_2{}^{18}O/H_2{}^{16}O$ ratio measurement. *Journal of Geophysical Research,* **87**, 5796-5808.

Flagg, C. N., M. Dunn, D. Wang, H. T. Rossby, and R. L. Benway, 2006: A study of the currents of the outer shelf and upper slope from a decade of shipboard ADCP observations in the Middle Atlantic Bight. *Journal of Geophysical Research - Oceans,* **111**, C06003.

Fogarty, M., L. Incze, K. Hayhoe, D. Mountain, and J. Manning, 2007: Potential climate change impacts on Atlantic cod (*Gadus morhua*) off the northeastern USA. *Mitigation Adaption Strategies Global Change,* **13**, 453–466.

Foley, A., P. Leahy, E. Mckeogh, 2010: Wind power forecasting & prediction methods. Conference on Environment and Electrical Engineering, 9.

Franchito, S., V. Rao, J. Stech, J. Lorenzzetti, 1998: The effect of coastal upwelling on the sea-breeze circulation at Cabo Frio, Brazil: a numerical experiment. *Annales Geophysicae*, **16(7),** 866-871.

Gaertner, E. et al. 2020: Definition of the IEA 15-Megawatt Offshore Reference Wind. Golden, CO: National Renewable Energy Laboratory. NREL/TP-5000-75698.

Glenn, S. M., T.N. Miles, G.N. Seroka, Y. Xu, R.K. Forney, F. Yu et al. 2016: Stratified coastal ocean interactions with tropical cyclones. *Nature Communications,* **7**, 10887.

Glenn, S., et al. 2004: Biogeochemical impact of summertime coastal upwelling on the New Jersey Shelf. *Journal of Geophysical Research - Oceans,* **109**, C12S02.

Gong, D. J., J. T. Kohut, and S. M. Glenn, 2010: Seasonal climatology of wind-driven circulation on the New Jersey Shelf. *Journal of Geophysical Research,* **115**, C04006.

Houghton, R. W., R. Schlitz, R. C. Beardsley, B. Butman, and J. L. Chamberlin, 1982: The Middle Atlantic Bight Cold Pool: Evolution of the Temperature Structure During Summer 1979. *Journal of Physical Oceanography,* **12**, 1019-1029.

Ignatov, A., 2010: Advanced Baseline Imager (ABI) Algorithm Theoretical Basis Document for Sea Surface Temperature. NOAA NESDIS STAR.

Kempton, W., C. Archer, A. Dhanju, R. Garvine, and M. Jacobson, 2007: Large CO2 reductions via offshore wind power matched to inherent storage in energy end uses. *Geophysical Research Letter*, **34**, L2817.

Ketchum, B. H., and N. Corwin, 1964: The persistence of winter water on the continental shelf south of Long Island, New York. *Limnology and Oceanography,* **9**, 467–475.

Kohut, J. T., S. M. Glenn, and R. J. Chant, 2004: Seasonal current variability on the New Jersey inner shelf. J*. Geophys. Res.*, **109,** C07S07, doi:10.1029/2003JC001963.

LaCasse, K. M., M. E. Splitt, S. M. Lazarus, and W. M. Lapenta, 2008: The Impact of High-Resolution Sea Surface Temperatures on the Simulated Nocturnal Florida Marine Boundary Layer. *Mon. Wea. Rev.*, **136**, 1349–1372.

Lentz, S. J., 2017: Seasonal warming of the Middle Atlantic Bight Cold Pool. *Journal of Geophysical Research. Oceans,* **122**, 941-954.

Lentz, S., K. Shearman, S. Anderson, A. Plueddemann, and J. Edson, 2003: Evolution of stratification over the New England shelf during the Coastal Mixing and Optics study, August 1996–June 1997. *Journal of Geophysical Research - Oceans,* **108**, 3008-14.

Li, Xu., J. Derber, A. Collard, and S. Moorthi, 2018: Sea Surface Temperature analysis within the NCEP GFS. 19th GHRSST Science Team Meeting, Darmstadt, Germany.

Linder, C. A., and G. Gawarkiewicz, 1998: A climatology of the shelfbreak front in the Middle Atlantic Bight. *Journal of Geophysical Research: Oceans,* **103**, 18405-18423.

Lombardo, K. et al. 2018: Sensitivity of Offshore Surface Fluxes and Sea Breezes to the Spatial Distribution of Sea-Surface Temperature. *Boundary-Layer Meteorol,* **166,** 475–502.

MacKinnon, J. A., and M. C. Gregg, 2005: Spring Mixing: Turbulence and Internal Waves during Restratification on the New England Shelf. *Journal of Physical Oceanography,* **35**, 2425–2443.

Malone, T. C., L. H. Crocker, S. E. Pike, and B. W. Wendler, 1988: Influences of river flow on the dynamics of phytoplankton production in a partially stratified estuary. *Marine Ecology. Progress series (Halstenbek),* **48**, 235-249.

Manderson, J., L. Palamara, J. Kohut, and M. Oliver., 2011: Ocean observatory data are useful for regional habitat modeling of species with different vertical habitat preferences. Marine Ecology Progress, **438**, 1–17.

Maurer, J., 2002: Infrared and microwave remote sensing of sea surface temperature. University of Hawaii, Department of Aerospace Engineering Sciences. http://www2.hawaii.edu/~jmaurer/sst/.

Miles, T., G. Seroka, and S. Glenn, 2017: Coastal ocean circulation during Hurricane Sandy. Journal of Geophysical Research: Oceans, **122**, 7095–7114.

Minnett P.J. et al. 2019: Half a century of satellite remote sensing of sea-surface temperature. *Remote Sensing of Environment,* 233, 111366.

Mission Overview. NASA, GOES-R, https://www.goes-r.gov/mission/mission.html, (Accessed November, 20, 2020).

Mountain, D. G., and J. P. Manning, 1994: Seasonal and interannual variability in the properties of the surface waters of the Gulf of Maine. *Continental Shelf Research,* **14**, 1555-1581.

Münchow, A., A. K. Masse, and R. W. Garvine., 1992: Astronomical and nonlinear tidal currents in a coupled estuary shelf system. *Cont. Shelf Res*., **12(4),** 471–498.

Murphy, 2019: Exec. Order No. 92.

Narayan, N., A. Paul, S. Mulitza, and M. Schulz, 2010. Trends in coastal upwelling intensity during the late 20th century. *Ocean Sci*., **6 (3)**, 815-823

NBDC., 2009: Handbook of Automated Data Quality Control Checks and Procedures. NBDC Technical Document 09-02.

NJDEP, 2005: Potential Conflicts with Offshore Wind Projects. Retrieved from NJwindpanel.org.

NOAA. Why do scientists measure sea surface temperature? National Ocean Service website, https://oceanservice.noaa.gov/facts/sea-surface-temperature.html, 11/05/20.

Oliver, M., M. Breece, D. Fox, D. Haulsee, J. Kohut, J. Manderson, and T. Savoy, 2013: Shrinking the Haystack: Using an AUV in an Integrated Ocean Observatory to Map Atlantic Sturgeon in the Coastal Ocean. *Fisheries*, **38(5)**, 210-216.

O'Neill, L. W., D. B. Chelton, and S. K. Esbensen, 2010: The Effects of SST-Induced Surface Wind Speed and Direction Gradients on Midlatitude Surface Vorticity and Divergence. *J. Climate*, **23**, 255–281.

Optis, M. et al, 2020: Validation of RU-WRF, the Custom Atmospheric Mesoscale Model of the Rutgers Center for Ocean Observing Leadership. Golden, CO: National Renewable Energy Laboratory. NREL/TP-5000-75209.

Pacheco, A. L., 1988: Characterization of the Middle Atlantic Water Management Unit of the Northeast Regional Monitoring Plan. U.S. Dep. Commer., NOAA Tech. Memo. NMFS-F/NEC-56, 322.

Pryor, S.C. and Barthelmie, R.J., 2001: Comparison of potential power production at on- and offshore sites. *Wind Energ*., **4:** 173-181.

RFI-082, 2018: New Jersey Economic Development Authority. Port Infrastructure and Supply Chain Programs Supporting Offshore Wind Development**.**

Richaud, B., Y. Kwon, T.M. Joyce, P.S. Fratantoni, S. Lentz, 2016: Surface and bottom temperature and salinity climatology along the continental shelf off the Canadian and U.S. East Coasts. *Continental Shelf Research*, **124**,165-181.

Seroka G., E. Fredj, J. Kohut, R. Dunk, T. Miles, and S. Glenn, 2018: Sea Breeze Sensitivity to Coastal Upwelling and Synoptic Flow Using Lagrangian Methods. J. Geophys. Res. Atmospheres, **123**, 9443-9461.

Seroka, G., T. Miles, Y. Xu, J. Kohut, O. Schofield, and S. Glenn, 2016: Hurricane Irene sensitivity to stratified coastal ocean cooling. *Monthly Weather Review,* **144**, 3507–3530.

Schmit, T.J., P. Griffith, M.M Gunshor, J.M Daniels, S.J. Goodman, and W.J. Lebair, 2017: A Closer Look at the ABI on the GOES-R Series. *Bull. Amer. Meteor. Soc.,* **98,** 681–698.

Schwing F.B., M. O'Farrell, J.M. Steger, and K. Baltz, 1996: Coastal Upwelling Indices — West Coast of North America. NOAA, Technical Memorandum, 1946–95, NMFS NOAA-TM-NMFS-SWFSC-231.

Shabanov N., A. Ignatov, B. Petrenko, Y. Kihai and A. Heidinger, 2010: Towards integrated cloud mask and quality control for ABI SST product: prototyping with MSG/SEVIRI. NPOESS&GOES-R, 90-th AMS Annual Meeting, 17-21 January, Atlanta, GA.

Shah, H., S. Mathew, and C. M. Lim, 2015: Numerical simulation of flow over an airfoil for small wind turbines using the $\gamma-\mathrm{Re}\theta$ model. *International Journal of Energy and Environmental Engineering,* **6**, 419–429.

Smith, P. C., 1983: The mean seasonal circulation off southwest Nova Scotia. *Journal of Physical Oceanography,* **13**, 1034–1054.

Song, Q., T. Hara, P. Cornillon, and C. A. Friehe, 2004: A comparison between observations and MM5 simulations of the marine atmospheric boundary layer across a temperature front. *J. Atmos. Oceanic Technol*., **21**, 170–178.

Voynova, Y. G., M. J. Oliver, and J. H. Sharp, 2013: Wind to zooplankton: Ecosystem-wide influence of seasonal wind-driven upwelling in and around the Delaware Bay. *Journal of Geophysical Research. Oceans,* **118**, 6437-6450.

Wallace, E. J., L. B. Looney, and D. Gong, 2018: Multi-decadal trends and variability in temperature and salinity in the Mid-Atlantic Bight, Georges Bank, and Gulf of Maine. *Journal of Marine Research,* **76**, 163-215.

Wentz, F., C. Gentemann, D. Smith, D. Chelton, 2005: Satellite Measurements of Sea Surface Temperature Through Clouds. *Science,* **288**, 5467: 847-850.

Xie, Shang-Ping, 2018: Ocean-Atmospheric Interaction and Tropical Climate. International Pacific Research Center and Department of Meteorology, University of Hawaii.